TAMPEREEN TEKNILLINEN YLIOPISTO
TAMPERE UNIVERSITY OF TECHNOLOGY

PÖLÖNEN VILLE-MATTI

DESIGN OF BATTERY MODULE TESTER

Master of Science Thesis

Examiner: Ph. D Jenni Rekola
Examiner and topic approved by the Faculty Council of the Faculty of Computing and Electrical Engineering on 30th August 2017

ABSTRACT

Ville-Matti Pölönen: Design of Battery Module Tester
Tampere University of Technology
Master of Science Thesis, 56 pages, 10 Appendix pages
June 2018
Master's Degree Programme in Electrical Engineering
Major: Power Electronics
Examiner: Ph. D Jenni Rekola

Keywords: active rectifier, battery, battery charger, battery management system, buck converter, cascade control, separate control, optocoupler

Diesel use as fuel is decreasing due to climate change. New replacement power sources are hybrid and fully electric uses to minimize carbon dioxide emissions. The battery modules, which are used for these applications, need to be tested to guarantee their proper operation. The actual testing procedure is not in the scope of this thesis.

The main targets are to compare different alternatives for the power supply, implement the control system and choose the most suitable solution to this study. The maximum power is *75 kW* which creates its own challenges to component design. The main parameters are voltage and current. The input fuse, which is connected straight to the grid, must be at least *100 A* since the maximum charging and discharging current for the battery modules is *600 A* while voltage of the battery modules varies within *24 VDC* and *125 VDC* depending on the amount of battery modules in series. Isolation from the main grid is important because of harmonics and filtering the common-mode noise. The power flow can be unidirectional or bidirectional in grid perspective. Three alternatives for the power supply structure and control are presented in this thesis.

Since batteries are used, accurate control is a challenge for voltage is low and current high. The control needs to be done carefully, to achieve a stable system. Temperature is a very critical factor, because of lithium-ion batteries. Current and voltage supplied to the battery modules have to be limited on a level which is approved by the manufacturer.

Conventional battery chargers have a constant-voltage constant-current (CCCV) charging method. There are normally two stages in this charging method, the constant current -phase is applied for most of the charging and as the battery capacity increases close to its maximum, the constant voltage -phase is applied to load the battery fully. Since the tests which are done to the battery modules are based on varying the current reference, only the constant-current charging method with changing reference is deployed. The target is not to charge the battery modules fully, but rather adjust the current.

The thesis starts with an introduction in chapter 1, followed by battery modeling in chapter 2. Batteries are studied in a relevant manner to introduce problems and characteristics in control perspective. Different topologies are considered for the AC-DC interface in chapter 3 and control of the battery module tester is introduced in chapter 4. The control chapter includes pulse-width modulation (PWM), PID-controller and feedback systems. The justifications of the simulation model and component dimensioning are presented in chapter 5. All components used are chosen according to the calculations

presented in this thesis. Chapter 6 is about practical issues related to the battery module tester including an optocoupler coupling example and controller design. The last chapter is conclusions wrapping the whole thesis in couple of pages in chapter 7.

Initially, the battery module tester was planned to build during thesis, but this part is postponed due to lack of time. The buck converter topology is the best choice for the voltage regulation from AC voltage to controlled DC voltage since the control is simple, the price is lowest among the other alternatives and the power quality to the batteries is good without any additional filters provided that the passive components are large enough in the buck converter. It is possible to use multiple buck converters in parallel to reduce electromagnetic interference (EMI) and the stress on the components, but this requires accurate synchronization between the active switches, i.e. the switches should be on and off at the same times.

The control method is separate controllers for the output voltage and the output current, which is done by a programmable logic controller (PLC). The cascade control would be faster, but it would require a very accurate model of the battery modules which is very hard to achieve. There is only one reference value in cascade control, which disqualifies this option. The control method is discussed more in chapters 3 and 5.

TIIVISTELMÄ

Ville-Matti Pölönen: Akkumoduulitesterin suunnittelu
Tampereen teknillinen yliopisto
Diplomityö, 56 sivua, 10 liitesivua
Kesäkuu 2018
Sähkötekniikan diplomi-insinöörin tutkinto-ohjelma
Pääaine: Tehoelektroniikka
Tarkastaja: tohtori Jenni Rekola

Avainsanat: akku, akkulaturi, aktiivinen tasasuuntaaja, akunhallintajärjestelmä, buck-hakkuri, erillissäätö, kaskadisäätö, optoerotin

Dieselin käyttö polttoaineena vähenee johtuen ilmastonmuutoksesta. Uusia korvaavia teholähteitä ovat hybridikäytöt sekä täysin sähköistetyt käytöt, jotka minimoivat hiilidioksidipäästöjä. Akkumoduuleja, joita käytetään näihin käyttöihin, tarvitsee testata taatakseen niiden oikea toiminta. Varsinaiset testausmenetelmät eivät ole tämän työn laajuudessa.

Työn päätavoitteina on vertailla eri vaihtoehtoja akkumoduulien tehonlähteeksi, toteuttaa ohjaus and valita näistä sopivin vaihtoehto. Maksimiteho on *75 kW*, mikä asettaa omat haasteensa ohjaamiselle sekä komponenteille. Tärkeimmät parametrit ovat jännite ja virta. Sisääntulon sulakkeen, joka on kytketty suoraan verkkovirtaan, tarvitsee olla vähintään *100 A*, sillä maksimi lataus- ja purkuvirta ovat *600 A*, kun jännite vaihtelee välillä *24–125 VDC*, riippuen montako akkumoduulia ladataan tai puretaan. Galvaaninen erotus syöttävästä verkosta on tärkeää harmonisten yliaaltojen ja yhteismuotohäiriöiden takia. Tehon syöttö voi olla yksi- tai kaksisuuntainen verkon näkökulmasta. Kolmea eri vaihtoehtoa on verrattu teholähteeksi tässä työssä.

Koska ollaan tekemisissä akkujen kanssa, tarkka säätö on haaste, sillä jännite on matala ja virta on korkea. Ohjaus tarvitsee suunnitella tarkasti, jotta päästään stabiiliin ohjausjärjestelmään. Lämpötila on kriittinen tekijä Li-ion akkujen takia. Virta ja jännite, joita syötetään akkumoduuleille, tarvitsee rajoittaa tasoille, jotka valmistaja on ilmoittanut.

Tyypilliset akkulaturit käyttävät vakiojännite, vakiovirta – latausta. Yleensä tässä latausstrategiassa on kaksi eri tilaa, vakiovirta-vaihe kestää lähes koko latauksen, kunnes akun varaus nousee lähelle maksimiaan, jolloin säätö muuttuu vakiojännitealueelle. Vakiojännitteelle saadaan ladattua akku täyteen. Akkumoduuleille tehtävissä testeissä on tarkoitus säätää virtaa, joten ainoastaan vakiovirta-latausta käytetään tässä työssä asetusarvoa vaihtelemalla. Tarkoitus ei ole ladata akkumoduuleja täyteen, vaan säätää virtaa.

Työ alkaa johdannolla kappaleessa 1, jonka jälkeen akkuja on mallinnettu kappaleessa 2. Erilaisia topologioita on vertailtu AC-DC – rajapintaan kappaleessa 3 ja akkumoduulitesterin säätö on esitelty kappaleessa 4. Säätökappaleeseen sisältyy pulssinleveysmodulaatio (PWM), PID-säädin ja takaisinkytkentä. Teoriat simulointien takana ja komponenttien mitoitukset ovat esitetty kappaleessa 5. Kaikki komponentit, joita käytetään akkumoduulitesterin rakennuksessa, on mitoitettu tämän työn mukaisesti. Kappale 6 on käytännönläheisistä asioista liittyen akkumoduulitesteriin, kuten optoerotin esi-

merkki ja keskustelua elektromagneettisesti yhteensopivuudesta (EMC). Viimeinen kappale kietoo ympärilleen koko työn sisällön kappaleessa 7.

Alun perin tarkoitus oli rakentaa myös akkumoduulitesteri suunnittelun ohella, mutta ajan puutteen takia rakentamista siirretään. Tässä tapauksessa paras vaihtoehto on jännitettä laskeva buck-hakkuri, sillä jännitteensäätö AC-jännitteestä ohjatuksi DC-jännitteeksi on yksinkertaista, hinta on alhaisin vaihtoehdoista, ja akuille syötetty sähkönlaatu on melko hyvää ilman suurempaa erillistä filtteriä, olettaen että passiiviset komponentit buck-hakkurissa ovat tarpeeksi suuria. On myös mahdollista käyttää useampaa buck-hakkuria rinnan, jotta sähkömagneettista häirintää (EMI) ja komponentteihin kohdistuvaa rasitusta saadaan pienennettyä, mutta tämä vaatii aktiivisten kytkimien synkronisointia. Toisin sanoen, kytkinten tulisi olla päällä ja pois päältä samaan aikaan.

Ohjaustapana käytetään erillisiä säätimiä ulostulojännitteelle ja -virralle, jonka toteuttaa ohjelmoitava logiikka (PLC). Kaskadisäätö olisi nopeampi, mutta vaatisi todella tarkan mallin akkumoduuleista, jota on hankala mallintaa. Kaskadisäädin käyttää vain yhtä varsinaista vertailuarvoa, mikä sulkee pois tämän vaihtoehdon. Säädöstä on keskusteltu enemmän kappaleissa 3 ja 5.

PREFACE

The initial thought of doing this thesis first occurred in July 2017 while I was still working at Kalmar as a summer trainee. As a post-job, the thesis was done by spring 2018.

I would like to thank Mikko Nurmela, Ville Kaivo, Juuso Kukkaro and Henrik Häggblom for the opportunity of doing this thesis and for the guidance along the way.

In Tampere, 17.5.2018

Ville-Matti Pölönen

CONTENTS

1. INTRODUCTION 1
2. MODELING OF LI-ION BATTERY MODULE 3
   2.1 Fundamentals of battery 3
   2.2 Battery modeling 5
   2.3 Battery management system 6
3. COMPARISON OF CONVERTER TOPOLOGIES AND CONTROL METHODS 8
   3.1 Option 1: Buck converter 8
      3.1.1 ”Constant current – constant voltage” –control 10
      3.1.2 Cascade control 11
   3.2 Option 2: Active rectifier 13
   3.3 Option 3: Battery chargers in parallel 15
   3.4 Discussion about the alternatives 16
4. CONTROL OF BATTERY MODULE TESTER 18
   4.1 System representation 18
   4.2 Feedback-control 20
   4.3 Pulse-width modulation of DC-DC converters 23
5. BUCK ANALYSIS 25
   5.1 Component selection 25
   5.2 Separate controller 30
      5.2.1 Voltage-fed voltage-output mode 31
      5.2.2 Voltage-fed current-output mode 35
   5.3 Cascade control 41
6. PRACTICAL DESIGN OF BATTERY MODULE TESTER 45
   6.1 Programmable logic control 45
   6.2 Optocouplers 47
7. CONCLUSIONS 51
8. REFERENCES 53

REFERENCE A: Buck calculations (VFVO)

REFERENCE B: Buck calculations (VFCO)

TERMS AND DEFINITIONS

AC	Alternating current
BMS	Battery management system
CB-PWM	Carrier-based pulse width modulation
CCCV	Constant current constant voltage
CPU	Central processing unit
DC	Direct current
DOD	Depth of discharge
DSP	Digital signal processor
EMC	Electromagnetic compatibility
EMI	Electromagnetic interference
ESL	Equivalent series inductance
ESR	Equivalent series resistance
IGBT	Insulated gate bipolar transistor
LED	Light emitting diode
LHP	Left-half plane
MOSFET	Metal-oxide-semiconductor field-effect-transistor
OCV	Open circuit voltage
PCB	Printed circuit board
PLC	Programmable logic controller
PWM	Pulse width modulation
RHP	Right-half plane
SOC	State of charge
VFCO	Voltage-fed current output –mode
VFVO	Voltage-fed voltage output –mode

C	Capacitance
D	Duty ratio
f_s	Switching frequency
G_{cc}	Current controller transfer function
G_{co}	Control-to-output transfer function
G_{cv}	Voltage controller transfer function
H_d	Sensing gain
I	Current
I_o	Load/output current
i_C	Collector current
i_L	Inductor current
K	Coefficient for controller
L	Inductor
R	Resistance
Rs	Sensing resistor gain
r_C	ESR of capacitor
r_d	Diode resistance
r_L	ESR of inductor
r_s	Battery impedance
r_{sw}	Switch resistance
T_s	Time period
U	Voltage

$u_{control}$	Modulating signal
u_{tri}	Carrier signal
V_{BE}	Base-to-emitter voltage
V_D	Diode voltage
V_{DS}	Drain-to-source voltage
V_{GS}	Gate-to-source voltage
V_{in}	Input voltage
V_o	Output voltage
V_T	Threshold voltage
$v_{c,in}$	Input capacitor voltage
$v_{c,out}$	Output capacitor voltage
w_p	Angular frequency of pole
w_z	Angular frequency of zero.

1. INTRODUCTION

As the conventional power sources tend to be not environment-friendly, hybrid and fully electric uses are becoming more popular alongside with batteries. Diesel has been the conventional source of power in harbor use, but due to the climate change, actions have been taken to diminish CO_2 –emissions. According to the standards, any high-power appliance including batteries is not allowed to use before standardized tests. The battery module tests can be subcontracted but because of special devices and knowledge is required, the costs of those tests are high. Therefore, the company is interested in building up their own battery module tester to perform the tests on their own.

The battery modules which are tested are in the voltage range of *24 V – 125 V,* Li-ion batteries, and in case of batteries all currents and voltages are DC. These modules are used as an optional or main power supply because some of the products use also diesel as power source. In these battery tests, the current is varied within *50 A* and *600 A*. *360 A* is the maximum continuous discharge or charge current according to the manufacturer, but *600 A* is the maximum pulsating current for *10 s*. The tests involve charging and discharging so the direction of supply in battery perspective varies within a test. One battery module has a nominal voltage of *24 V* and the battery module tester should be able to run a test up to 5 modules in series limiting the maximum nominal voltage to *125 V*.

The battery modules include battery management systems (BMS) logging knowledge of cell voltages, temperatures and state-of-charge (SOC). This is important for control, since if temperature or voltage of any cell is too high the power supply needs to be stopped. Other BMS functions, such as cell balancing, are described in their own chapter 2.3. The power supply from the grid can be implemented by using a commercial DC-power supply, an active rectifier or a self-made power converter such as buck converter.

The schematic structure of the power supply is shown in Figure 1. AC voltage from the grid is rectified to DC voltage using a passive 6-pulse diode bridge or directly to adjustable DC voltage with an active rectifier. If the diode bridge is used, the next step is to control the battery current according to current/voltage reference so that the battery current is adjusted to a level what the controller determines. The batteries determine the limits for the controller to avoid overloading. Two functions need to be considered; first how to implement protection for the batteries and the second is how to design the controller to be able to adjust current either unidirectionally or bi-directionally. The battery modules are connected via CAN-bus to the PLC which is the controller and thus it must

be able to control the power flow and in a hazardous situation to be able to power off the battery modules.

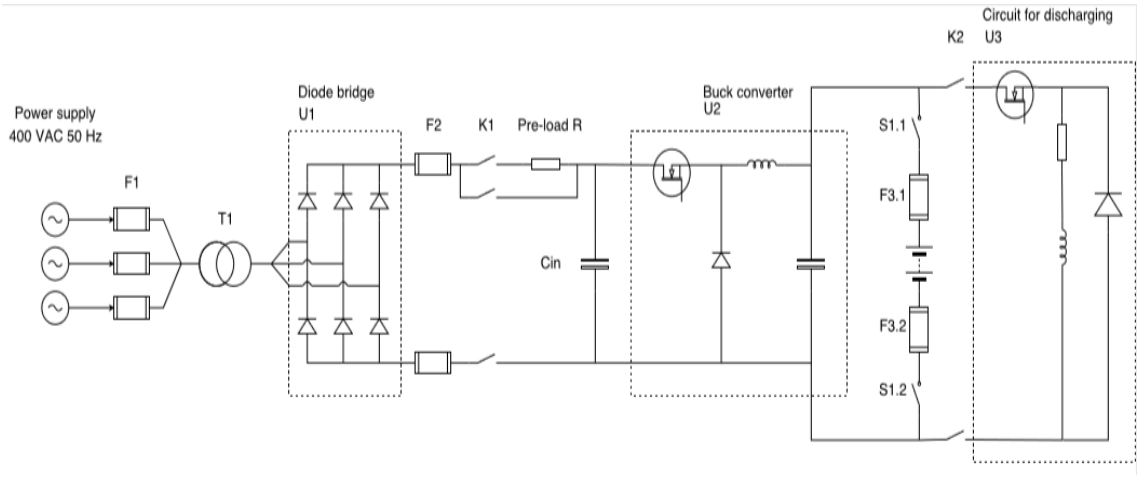

Figure 1. Schematic diagram of battery module tester.

The fuses in Fig. 1 are responsible for the primary protection while the PLC is responsible for the secondary protection according to the BMS states, such as overvoltage or overtemperature. The fuses *F1* are used for protection against faults in the grid, *F2* for failures in the DC-side and *F3* to protect the batteries. The transformer has a conversion factor of 3,2, allowing the converter input voltage to be roughly *170 VDC* and providing galvanic isolation from the main grid. The contactors *K1* are used for pre-loading the capacitors used in the DC-side. The pre-loading is done first via a resistor and when the capacitors are fully charged the lower contact is utilized to by-pass the resistor. The discharging of the batteries can be implemented to an external circuit or back to the grid.

The structure for the thesis is as follows: theory, design and building. In the theory part, related basics of batteries and control are covered. In the designing part different options are compared to each other, simulations and sizing of components are done. The last part is to tune the controller and condense the main issues related as conclusions. The core issue is designing the controller.

The practical implementation of the battery module tester is not included into this study due to lack of time and resources. However, all the components are dimensioned and the simulations are done including practical knowledge of the whole process.

2. MODELING OF LI-ION BATTERY MODULE

The fundamentals related to batteries and their features are described in this section. The objective is to have a model that can be used later to simulate the behavior of the battery. Furthermore, a basic description regarding batteries, especially Li-ion batteries, and their control system is introduced.

2.1 Fundamentals of battery

Batteries are generally divided into two groups: primary and secondary batteries. The primary batteries are non-rechargeable and thus the focus in this thesis is not on them. Li-ion batteries are an example of the secondary batteries and are especially the target of this section. To avoid confusion, the secondary batteries are rechargeable.

A battery consists of one or more cells. The cell consists of an anode, a cathode and an electrolyte. The anode is a negatively charged electrode and it supplies electrons via an external circuit in discharging (oxidation) to the cathode and accepts electrons in charging (reduction). Li-ions flow from the anode to the cathode in discharging and the other way around during charging while electrons flow from the anode to the cathode in discharging and vice versa in charging. The oxidation is generally loss of electrons and the reduction is gain of electrons. The cathode is a positively charged electrode and it acts reversibly compared to the anode. The movement of electrons in discharging is shown in Figure 2. [1]

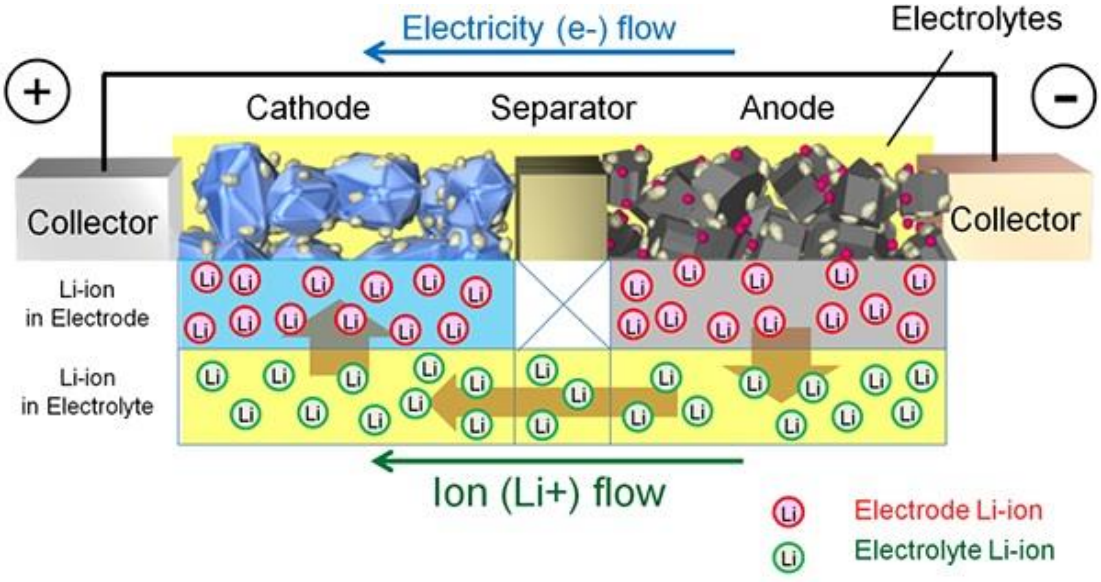

Figure 2. Li-ion battery during discharge [2].

The electrolyte is an ionic conductor, usually made of liquid, ions can move through it from the anode to the cathode or the other way around. Electrons cannot flow through the electrolyte, so electrons must be routed via an external circuit from the anode to the cathode in discharging, the electrolyte creates galvanic isolation between the electrodes. Furthermore, a separator is used to separate the anode and the cathode mechanically, however, it is permeable to the electrolyte. Current collectors are used for providing conductive path for electrons and to minimize resistance of the battery. Charging a battery is transforming electric energy to chemical energy and discharging is the reversible reaction. [1]

There are large number of battery chemistries like lead acid, lithium-ion, nickel metal hydride, nickel metal chloride, sodium sulfur, sodium chloride among other chemistries. These chemistries are divided into subclasses, in case of lithium-ion chemistries the most well-known are: lithium iron phosphate (LFP), lithium manganese oxide (LMO), lithium titanate (LTO), lithium cobalt oxide (LCO), lithium nickel cobalt aluminum (NCA) and lithium nickel manganese cobalt (NMC). Naturally, different chemistries have different properties. [3]

Today the focus is on lithium-ion batteries for their qualities are extra ordinary. If lithium-ion chemistries are not considered, then the sodium nickel chloride-based chemistries have the best characteristics regarding voltage (*2.6 V*) and specific energy (*100-120 Wh/kg*). Judging by specific power, nickel metal hydride chemistries have the highest value of *250-1000 W/kg*. Cycle life of non-lithium-based chemistries is from 300 cycles up to 2500 cycles. In comparison, even the lowest voltage of the lithium-ion chemistries (LTO) has a cell voltage of *2.2-2.3 V*. LFP has a cell voltage of *3.2-3.3 V* and specific power is up to *2400 W/kg*. Specific energies vary within *70-220 Wh/kg* between the chemistries. High specific energy indicates that the battery can supply moderate current for a long time while high specific power is used to describe that the battery can deliver higher currents usually for brief period. [3]

Li-ion batteries are used, for example, in electric vehicles and electrical energy storages. Advantages of li-ion batteries are vast including rechargeability, high power density, flat discharge rate, high thermal stability, long cycle life (>1000), low cost, high capacity and good low-temperature performance. There are also some disadvantages, such as degradation at high temperature, need for protective circuitry, capacity loss and potential for thermal runaway when overcharged. The best storage state-of-charge for Li-ion batteries is at *50 %* for phases of no use. The rate of loss of capacity decreases if the storage time increases. Pulse charging is also possible. One of the main drawbacks in lithium-ion batteries is that they have no tolerance of overcharging. Furthermore, all batteries consume materials in charging-discharging circles which means their capacity decreases over time. [1], [3]

The safe operation of li-ion batteries needs to be guaranteed. Potential hazardous situations exist, such as short-circuiting of battery terminals, excessive high rate discharge or charge, overdischarge or -charge, improper controller and imbalance between cells. Batteries must be protected from these conditions. Voltage, current and temperature of a cell or a battery should be kept in the specified area. Fuses can be used for short-circuit protection. Thermostats may be utilized to open battery circuit if temperature or current is too high. Protection devices can be installed to the circuit or within the battery pack, for example a fuse can be installed in series with the battery. Battery management systems are used for these functions in case of lithium-ion batteries.

2.2 Battery modeling

There are a lot of models for predicting the battery behavior. Some of these models are highly mathematical and some are very simple. The motive for battery modeling in this thesis is to have adequate accuracy for the simulations. Only equivalent circuit models [4] are described in this section.

The simplest model for batteries is the ideal model which is only a voltage source. This model does not consider current, so it is not usable. An improved model has a series resistance, i.e. the internal resistance of the battery added to the voltage source. This kind of model is called as the linear model [4] which is represented in Figure 3.

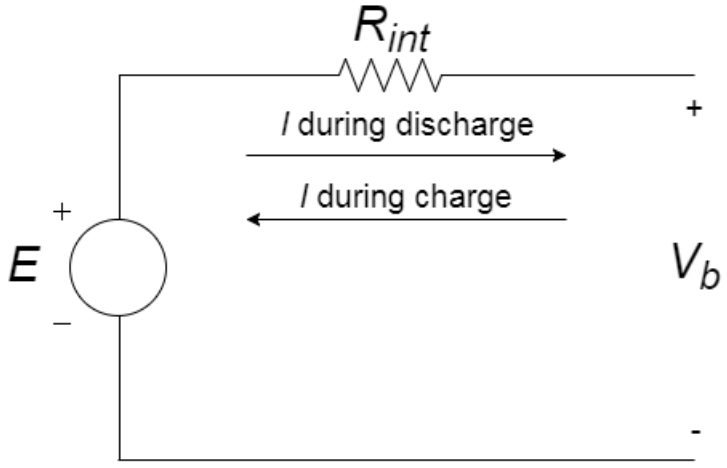

Figure 3. Linear model.

In this model E is the no load voltage of the battery, or the open circuit voltage of the battery, R_{int} is the internal resistance (impedance) of the battery and V_b is the battery voltage which depends on the current I. Current direction depends on whether the battery is being charged or discharged. R_{int} and E can be made dependent on the battery SOC in more accurate models. The battery voltage can be calculated based on Fig. 3 by Eq. 1.1.

$$V_b = E - R_{int}I \tag{1.1}$$

Where I is the discharging current of the battery in Eq. 1.1. If the battery was being charged the minus sign in Eq. 1.1 would be plus sign. The battery voltage depends on the initial open circuit voltage, the internal resistance of the battery and the discharging or charging current.

More accurate model is shown Figure 4. This model has two other parameters and it is called as the Thevenin model. C is the battery capacitance and R_{over} is the overvoltage resistance [4]. Even if this model is more accurate than the linear model, the parameters are not that easily available. Manufacturers usually report only on the internal resistance or impedance of the battery which suggests the use of linear model.

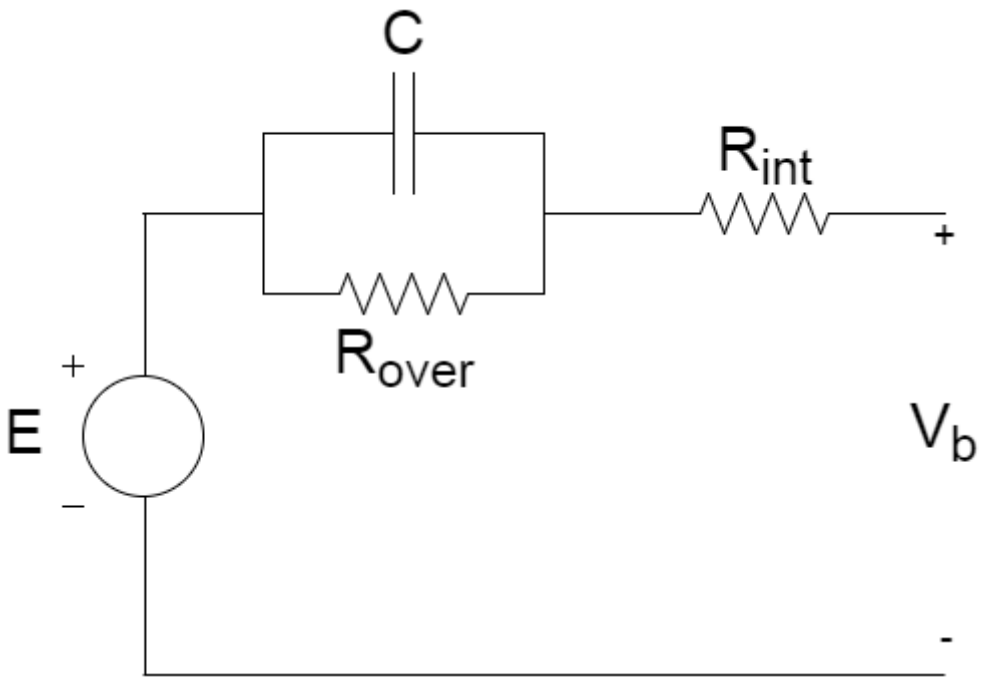

Figure 4. Thevenin model.

The linear model is more applicable since all the parameters are known. Even if the accuracy of the model is not perfect, the controller can be tuned using the linear model. After all, the controller determines the output for the controller uses closed-loop control allowing an accurate control result.

2.3 Battery management system

BMSs are used with Li-ion batteries, primarily to protect the batteries. The BMS monitors voltage, state of charge (SOC) and temperature [1]. More accurately, the BMS needs to limit voltage and current according to the safety levels defined by the manufacturer. In lithium-ion batteries the voltage of each individual cell is monitored and usually there is a secondary monitoring in case of failure in the primary monitor.

Balance must be kept between the cells in a battery for the cells heat up at different rate if there is imbalance between them. In case of an imbalanced battery, the lowest capacity cell determines the duration of the discharge and the highest capacity controls the capacity returned during the charge. Thus, the cells should have as identical capacities as possible or the cells should be balanced. Thermal runaway is possible to occur in case of abusive conditions, such as high current. [1], [5]

In practice, a BMS is a combination of host or master controller printed circuit board (PCB), a series of slave control boards, sensors and software. The BMS protects against overcharging, overdischarging, high temperatures, short circuiting and other failure modes. Other functionalities involve monitoring the state of the battery and its cells, balancing the cells and communication within the battery pack and to the outside controllers and systems. In an advanced BMS monitoring state of health (SOH) and SOC are involved in the BMS. The main functions for the BMS are to ensure safe operation and to optimize the lifetime of the battery. [5]

All in all, the calculations provided by the BMS can be difficult. For example, a voltage curve at different depth of discharge (DOD) is shown in Fig. 5. There are ranges of DODs during which the voltage stays constant. On the other hand, it is easy to see when the battery is close to its minimum/maximum DOD. The operation of the battery needs to be restricted since Li-ion batteries should not be overdischarged or -charged.

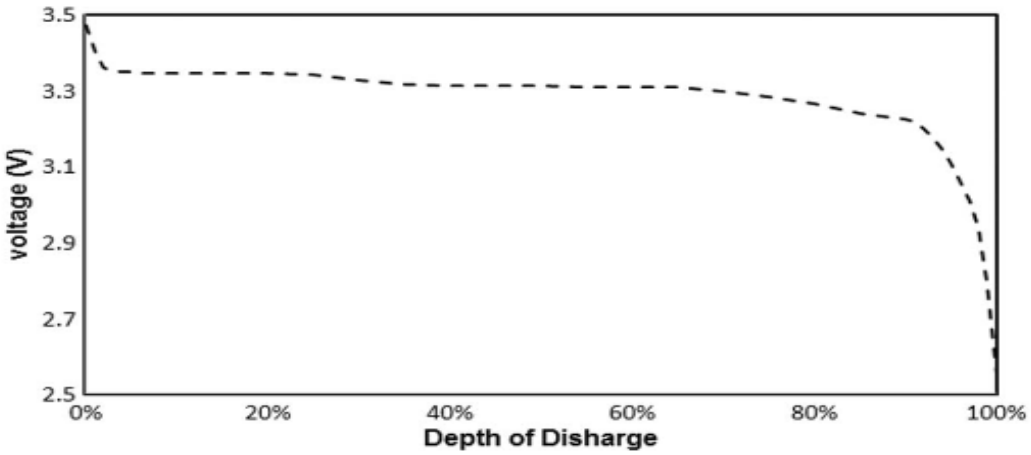

Figure 5. Discharge curve of nanophosphate Li-ion cell [6].

Each module is equipped with BMS in this application and the BMSs communicate via CAN-bus with the PLC. The BMSs provide the primary knowledge of the battery voltages and temperatures, but the PLC is also responsible for monitoring overvoltage and overcurrent. The PLC executes the current/voltage limiting.

3. COMPARISON OF CONVERTER TOPOLOGIES AND CONTROL METHODS

There is a lot of research and development regarding the battery technology nowadays for electric vehicles are rapidly generalizing, chemistries are evolving, and prices are coming down. Li-ion chemistry seems to be the best option, for now.

The power flow of the battery module tester can be either unidirectional or bi-directional. If the power flow is bi-directional the power quality must be good enough to the grid according to the standards. Thus, some filtering and bi-directional components, IGBT modules instead of diodes, are required.

The first option is a buck converter. In control perspective, it is possible to control the output with separate controllers 3.1.1 or cascade control 3.1.2. The second alternative is an active rectifier 3.2, and the last option would be to use commercial battery chargers in parallel 3.3. The actual controller is a PLC. The PLC ensures safe operation and can shut down the whole system in case of an error.

The battery modules, which are *24 VDC* Li-ion batteries, must operate safely and accurate by measuring the output voltage and the output current. Furthermore, the BMS of the modules provides information about the SOC of the batteries and temperatures. The minimum and the maximum ratings for voltage are defined by the manufacturer. Some safety margin is good to have, so around *0.5 V* from both ends, minimum and maximum, can be taken out.

3.1 Option 1: Buck converter

The buck converter topology is shown in Figure 6. The number of buck converters can be single or multiple which would be connected in parallel. However, the control strategy is divided into two options. A brief introduction to buck converters is shown here after which two different control strategies are reviewed.

AC-voltage is rectified into DC using a diode bridge and filtered with an input capacitor C_{in}. This voltage is then fed into the buck converter. The diode bridge is shown as an ideal DC-voltage source. Batteries are modeled using a voltage source and a series resistance, or internal impedance, of the battery which is *the linear model* described in 2.2.

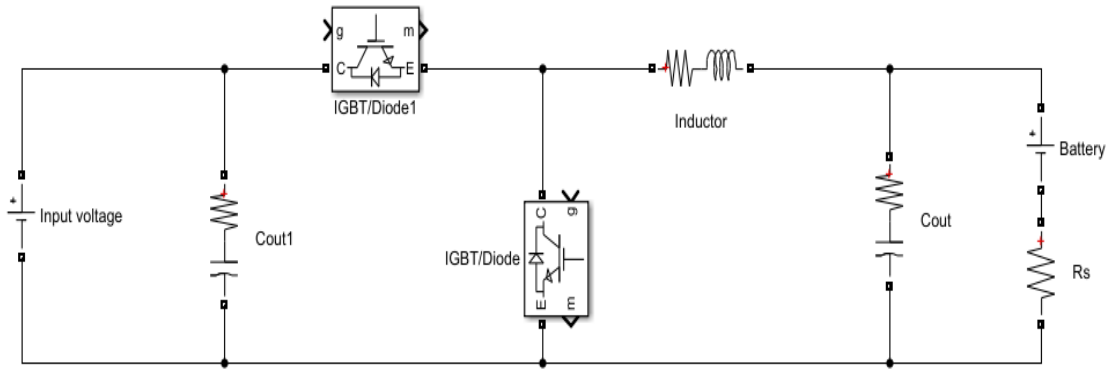

Figure 6. Buck converter.

In this configuration, the input voltage V_{in} is known and the battery current or voltage is assumed to be known based on the controlled output variable. The battery charger uses a voltage controller and a current controller; thus, both the output variables must be measured. The controller can be done controlling the output voltage u_o and the output current i_o separately or both at the same time, i.e. to use cascade control. The name VFVO [7] refers to voltage-fed voltage-output mode in which 'voltage-output' means that voltage is controlled, i.e. kept constant while VFCO stands for voltage-fed current-output mode in which current is controlled. As a summary, first voltage is controlled according to the reference value after which the controller changes to the current-output mode which keeps the current according to the reference value.

On-time circuit for buck-converter is illustrated in Figure 7 and off-time circuit in Figure 8. Both are needed so that the linearized state space can be solved eventually. The battery is modeled as a voltage source in Fig. 7 and Fig. 8, but it has a series resistance inserted inside the voltage source.

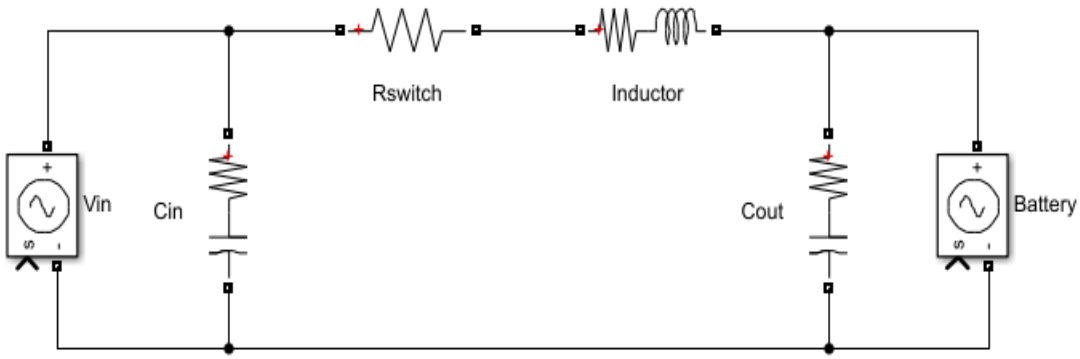

Figure 7. Buck on-time.

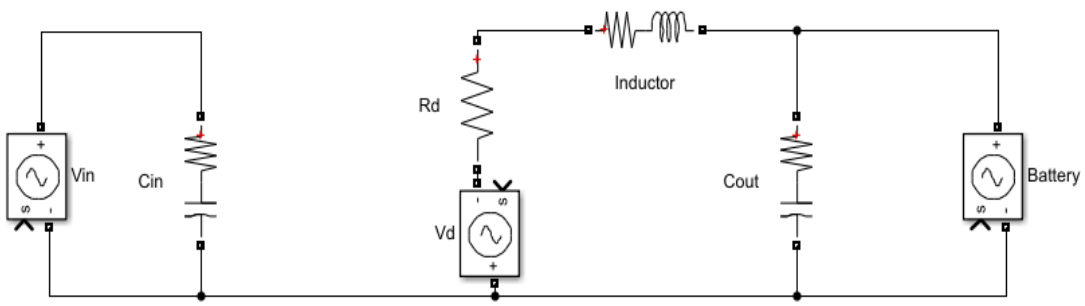

Figure 8. Buck off-time.

The state variables are the capacitor voltages $v_{c,in}$ and $v_{c,out}$ and the inductor current i_L for both VFVO- and VFCO-mode. The input variables are the input voltage and the output current for VFVO-mode while for VFCO-mode the input variables are the input voltage and the output voltage. Thus, the output variables are the input current and the output voltage or current depending on the mode used. All these variables are described in section 4.1. The equations are based on Kirchhoff's voltage and current laws. Key points in this analysis is to calculate the on- and off-time equations for the state and output variables, then average the state space using the calculated equations. After this step, the steady state operating point can be calculated by substituting the derivatives with 0. The last step is to use partial derivatives to achieve the linearized state space.

The detailed calculations are presented in appendixes A and B. In the analyses it has also been considered the load effect. This is done because otherwise the analyses would be ideal not considering the load and its features. The detailed mathematical analysis is not in the scope of this thesis, so a detailed explanation is not performed. However, the analysis is based on [7].

3.1.1 "Constant current – constant voltage" –control

The first used control system is based on conventional battery charger which uses constant current and constant voltage control schematics of which the constant current control is first used, and to charge batteries fully the constant voltage control is used i.e. constant current constant voltage (CCCV) controller. This control system is modified to change charging or discharging current continuously. This is achieved by changing reference voltage. An example of conventional battery charging voltage and current curves is shown in Figure 9.

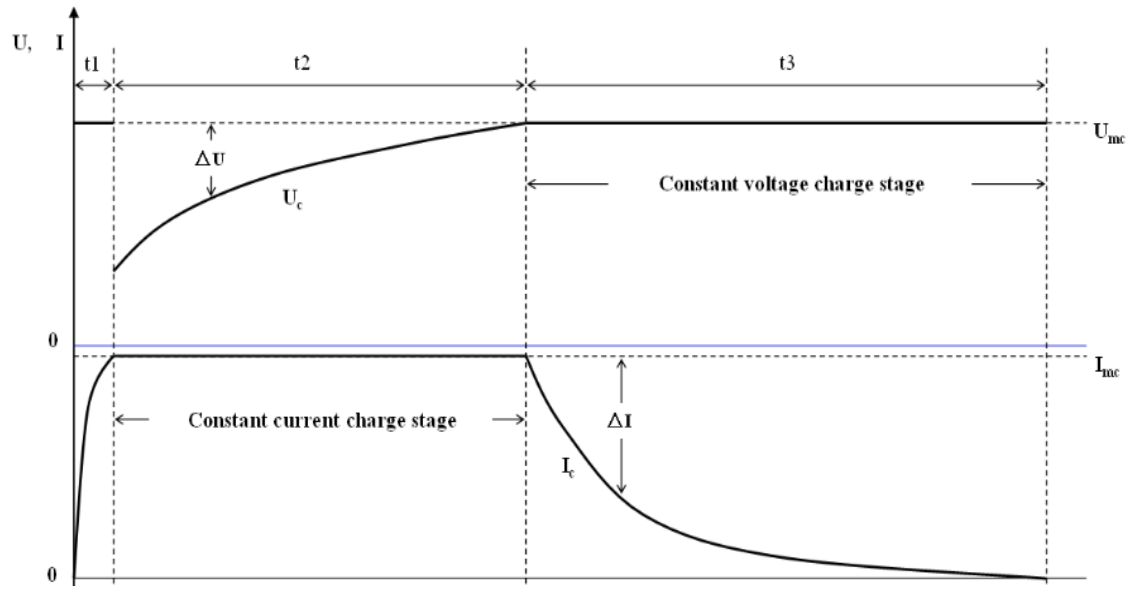

Figure 9. Constant current constant voltage -charging [8].

The procedure starts usually with pre-charge if the battery voltage is heavily discharged which is marked in Fig. 9 as t_1. This can be confirmed by comparing the battery voltage to minimum charging voltage limit or if the SOC is measured, this determines what is the current capacity of the battery. This period lasts until the minimum charging limit voltage is achieved. After this time a greater, constant current is supplied to the battery terminals which is called as the current-regulation phase or constant current phase t_2. The battery voltage is measured and the SOC is calculated which is the indicator of battery's current capacity. Near the full-charge voltage and SOC, the voltage regulation phase t_3 is entered, and the current starts to decrease rapidly. When the full-charge voltage is completely achieved the charging is finished and the charging current is close or equal to *0 A*. The charging can take from 10 minutes to many hours, depending on the capacity, charging capability, chemistry and control system. [9]

The constant current phase is applied when the battery voltage is less than the reference voltage, usually near the maximum voltage of the battery. If, on the other hand, the battery voltage is greater than the reference voltage constant voltage is applied. In the case of the battery module tester, only constant current charging is relevant since the target of the charging is not to charge batteries fully, but rather vary the discharging and charging currents. Because of the battery voltage which does not change rapidly excluding switching transient, it makes more sense to control voltage first and then keep current on a level which is set.

3.1.2 Cascade control

The alternative control approach for the buck converter is *cascade control*. Cascade control is based on indirect control, i.e. the controlled values are not controlled separately, but rather together and it improves the overall dynamics [10]. There is an inner loop

and an outer loop. In this version, the current controller is the inner loop and the voltage controller the outer loop. The inner loop needs to be controlled much faster, at least a decade should suffice in terms of crossover frequency, so that the outer loop can be controlled precisely. This kind of configuration yields such a result that current is indirectly controlled much faster while voltage is directly controlled but slightly slower.

This method could be implemented in accordance with Figure 10 if the battery model would be very accurate because this method relies on the output voltage reference, and the output current is the primary control variable. If the reference signal would be the output current the implementation would be very hard to realize for battery voltage does not change that rapidly and the inner loop needs to be faster than the outer loop.

The outer loop controls voltage, i.e. the reference voltage is compared to the measured output voltage. This signal is fed into PI-controller G_{cv} which is the reference signal for the current controller. The current controller compares this reference to the measured current, which in simulations is equal to duty ratio multiplied with the transfer function G_{co}^{I} which is the control-to-output transfer function. The control-to-output transfer functions are reviewed later in 5.2. ^{I} denotes to a current transfer function and ^{V} to a voltage transfer function. This signal is multiplied with sensing resistor gain R_s which is set to 0.1 and compared to the reference signal formed by the outer loop.

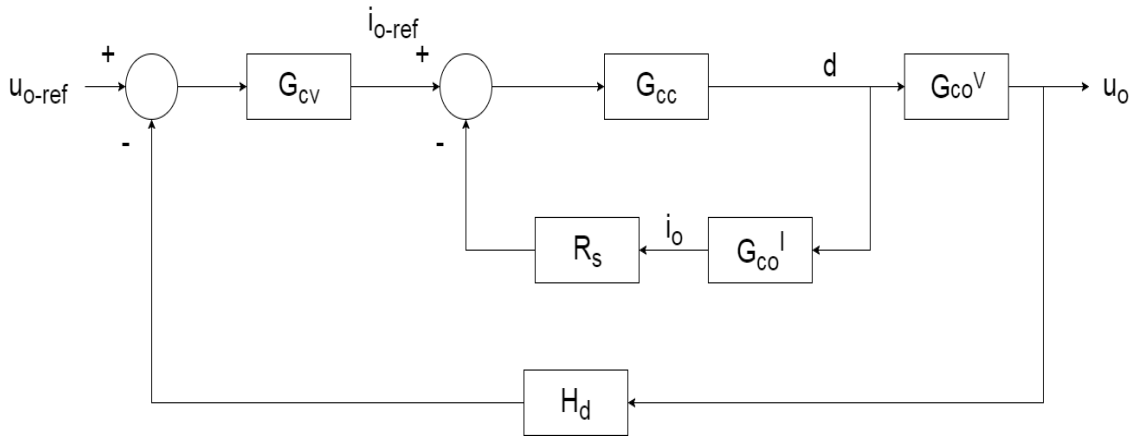

Figure 10. Control schematics.

H_d could be used for depicting a voltage divider, but in Fig. 10 H_d is equal to 1. Both sensing gains H_d and R_s are scaling factors which corresponds to the value of a current transformer or sensing resistor in case of current and resistor dividers in case of voltage. Two measurements need to be done, but only one reference value is required.

Loop gains consider all the transfer functions which are in a certain loop. The loop gain is equal to the products of the gains in the forward and feedback paths [11] and it can be open-loop or closed-loop, in this thesis all the loop gains are open-loops. The loop gains can be solved according to the transfer functions shown in Figure 10. The relationship between the duty ratio and the output current reference is calculated in Eq. 3.1.

$$\hat{d} = (\hat{\imath}_{o_{ref}} - R_s {G_{co}}^I \hat{d}) G_{cc}$$

$$\hat{d} + G_{cc} R_s {G_{co}}^I \hat{d} = G_{cc} \hat{\imath}_{o_{ref}}$$

$$\frac{\hat{d}}{\hat{\imath}_{o_{ref}}} = \frac{G_{cc}}{1 + G_{cc} R_s {G_{co}}^I} \tag{3.1}$$

This is the inner loop of the cascade control system. It is used for tuning the voltage controller in Eq. 3.2.

$$\hat{u}_o = \left(\hat{u}_{o_{ref}} - H_d \hat{u}_o\right) G_{cv} \frac{G_{cc}}{1 + G_{cc} R_s {G_{co}}^I} {G_{co}}^V$$

$$\hat{u}_o + H_d G_{cv} \frac{G_{cc}}{1 + G_{cc} R_s {G_{co}}^I} {G_{co}}^V \hat{u}_o = G_{cv} \frac{G_{cc}}{1 + G_{cc} R_s {G_{co}}^I} {G_{co}}^V \hat{u}_{o_{ref}}$$

$$\frac{\hat{u}_o}{\hat{u}_{o_{ref}}} = \frac{G_{cv} \frac{G_{cc}}{1 + G_{cc} R_s {G_{co}}^I} {G_{co}}^V}{1 + H_d G_{cv} \frac{G_{cc}}{1 + G_{cc} R_s {G_{co}}^I} {G_{co}}^V} \tag{3.2}$$

Loop gains have an open-loop nature and can be used for tuning controllers. Using this kind of control strategy, the loop gains are in Eq. 3.3 and in Eq. 3.4.

$$L_c = G_{cc} R_s {G_{co}}^I \tag{3.3}$$

$$L_v = G_{cv} \frac{G_{cc}}{1 + G_{cc} R_s {G_{co}}^I} {G_{co}}^V H_d \tag{3.4}$$

These equations are used for tuning the controller in simulation chapter 5.3, but the transfer functions are shown in Figure 10, so the loop gains are shown here for convenience. It should be noted that the cascade control requires two measured feedbacks and one reference signal.

3.2 Option 2: Active rectifier

Another option is to use an active rectifier which can convert AC to DC, and it is shown in Figure 11. The control strategy would be implemented with cascade control. A diode is added in parallel to each IGBT since IGBTs cannot tolerate reverse voltage. Usually these diodes are called a freewheeling diode or fast recovery diode. The antiparallel diode is added to conduct reverse current. Inductive load can generate high voltage spikes which do not have a route if the antiparallel diode is not used, eventually destroying the power switch.

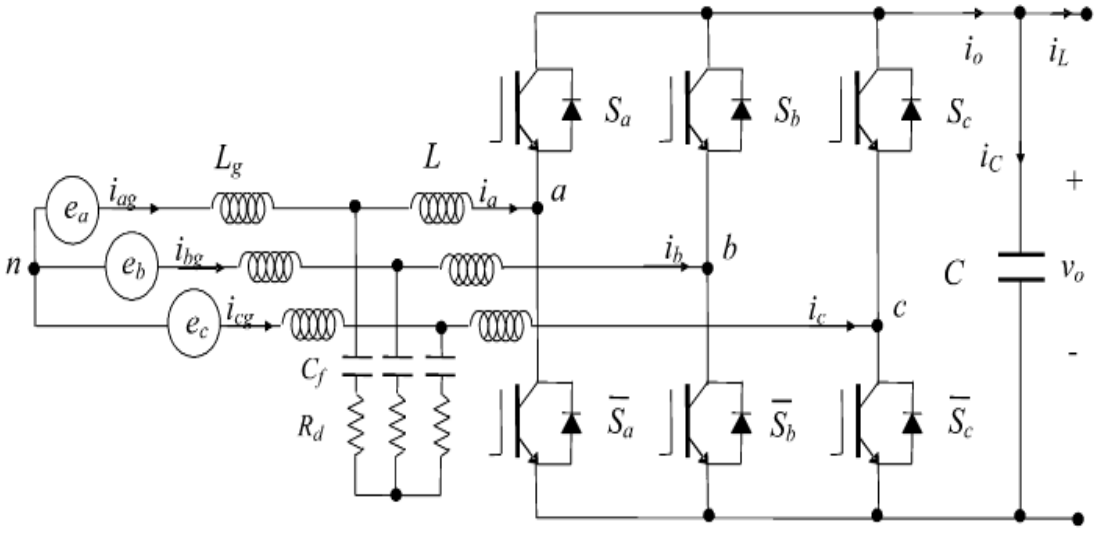

Figure 11. Active rectifier [12].

In this configuration it is possible to charge and discharge the battery bi-directionally. The dc-voltage is kept at a desired value, using feedback control and voltage reference. The error signal between measured dc link voltage and the reference voltage is used to switch to control the six switches. Because the current level is high and, thus, high input inductance is very useful to reduce current harmonics around the switching frequency. Without the filter, the power flow should be unidirectional. The LCL-filter is used to strengthen the power quality by reducing the switching frequency harmonics and differential mode EMI. [12]

Since the active rectifier would be bi-directional, the current flowing to the battery must be in phase with the output voltage of the rectifier (rectifier mode) during charging and during discharge the phase shift is *180°* (inverter mode) in grid perspective [13]. Furthermore, a modulation scheme, such as carrier-based PWM, which is suited for AC/DC or DC/AC control, should be used. In case of three-phase rectifier/inverter, each phase has its own modulating signal and the modulating signals have phase shift of *120°*. Each phase has 2 IGBTs connected in series and these switching devices have a phase shift of *180°* for the modulating signals. The modulating signals are compared to the carrier signal which is the same for all phases. The modulating factor *m* can be controlled which in turn controls the duty ratio besides the active and the reactive power can be controlled [14]. As in DC-DC converters, duty ratio controls the output quantities in AC-DC and/or DC-AC converters.

The power flow of a single leg is shown in Figure 12. The conduction path changes according to the direction of the current but the phase voltage remains unaffected.

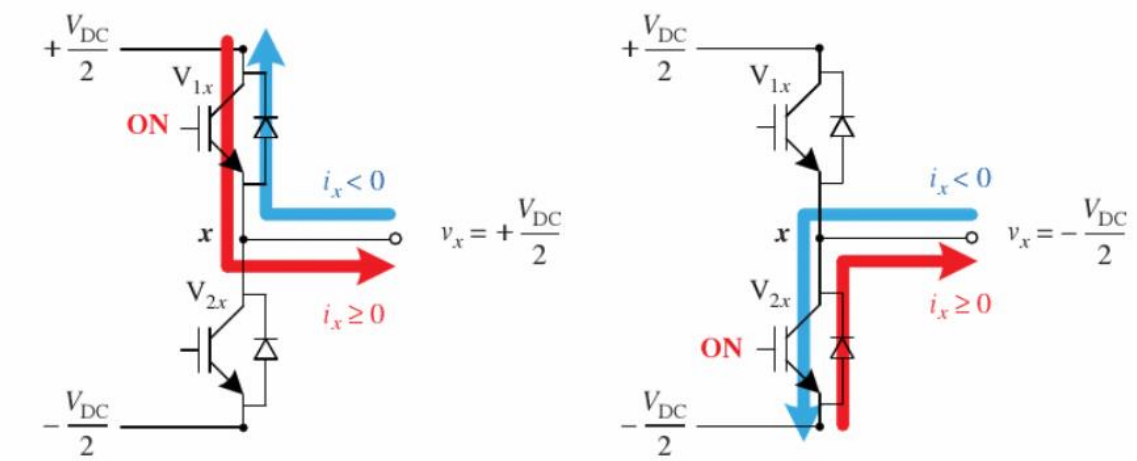

Figure 12. Switching sequence of a phase leg [15].

The voltage pulse widths produced by PWM are varied in terms of frequencies and voltages. There are plenty of PWM schemes, but the two most common are sinusoidal PWM (SPWM) and space vector modulation (SVM). Modulation index is the ratio of the reference voltage and the carrier signal. The maximum modulation index is 1 for SPWM and 1.15 for SVM in the linear range. If the SPWM is considered for three-phase inverter, the maximum line-to-line AC-side RMS voltage is Eq. 3.5 [16].

$$u_{LL\_rms\_max} = 0.61\, u_{dc} \tag{3.5}$$

The maximum DC voltage should be *170 VDC* which would require a line-to-line voltage of *103.7 VAC*$_{RMS}$. The phase voltage would be approximately *60 V*. The current handling capability for the IGBTs should be *390 A*, if 5 battery modules were connected in series and the maximum output power was *70 kW*. This would require a specific transformer, which most likely would not be a finished product. In practice, a buck converter would still be required before the battery modules if this option was used.

3.3 Option 3: Battery chargers in parallel

The last option introduced in this thesis is to use commercial battery chargers which are connected in parallel straight to the grid voltage. These chargers are usually powered by AC voltage and are capable of AC-DC -conversion as inverters. There are commercially available chargers which can be connected straight to one-phase *230 VAC*, *50 Hz* -supply and can produce *200 V* output voltage [18].

Electrical wiring diagram of the option 3 is presented in Figure 13. An adequate number of battery chargers is used to achieve the maximum current *600 A* and the voltage should be sufficient, up to around *125 V*. The discharging circuit is similar as in the case of buck converter.

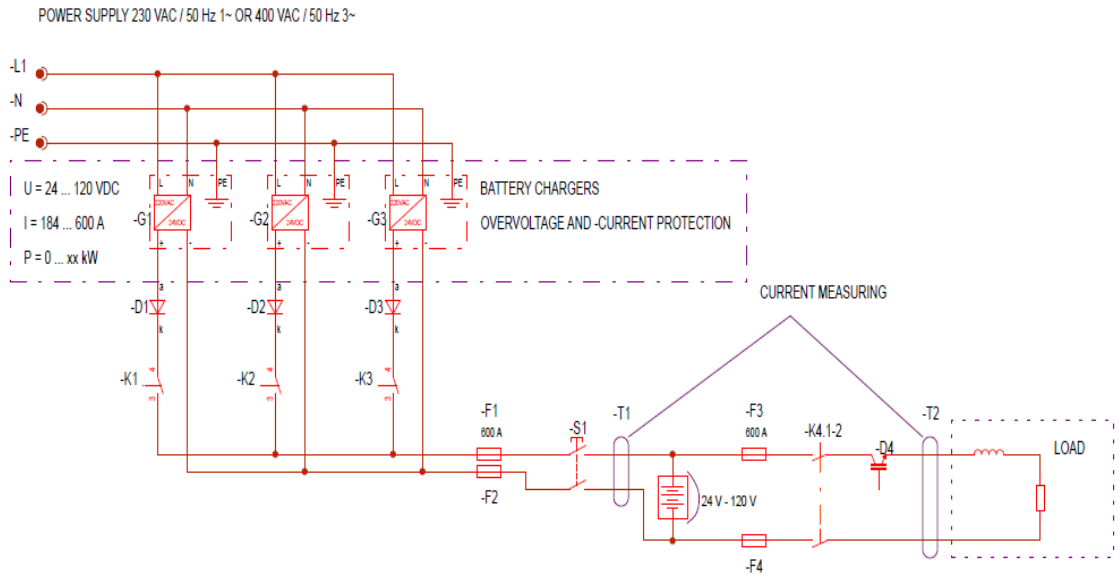

Figure 13. Wiring diagram of battery chargers.

The number of components depends on the power ratings of a single battery charger in this alternative. Each charger should be equipped with a diode to avoid short-circuiting. The voltage level should be from *20 V* up to *125 V* for one charger since all the chargers are parallel which means the voltage is similar between the chargers. Contactors are used to match the current demand. If the chargers can be idling even if they are connected, then the connectors are not needed. The output current and voltage should be measured, and the control can be done by the PLC.

Usually these devices are limited to low power levels, for example the most powerful device in [18] is only able to provide *3200 W* output power which would mean that in the real implementation there would be at least 21 of these modules. These modules can also be controlled via PC, which might be simpler than the control implemented in the PLC.

3.4 Discussion about the alternatives

Commercial battery chargers would be the simplest of the alternatives, but to gain a total current of *600 A* it would require 21 chargers assuming one charger can deliver the output power of *3200 W* in the required voltage range. The total cost of these chargers is not known, besides the space required would be large. However, these chargers have their protection and are EMC-compatible. For example, Tesla Roadster is powered by 6831 individual Li-ion cells which is safer option than one very large battery [17]. Most manufacturers do not announce officially even their all their products, let alone the price of the devices [18].

The active rectifier would be useful since the diode bridge would not be needed and the grid voltage could be straight rectified to DC-voltage. The adjustability of this DC-

voltage would not be sufficient, so the buck converter would still be required. Power could be transmitted bi-directionally. However, this requires filtering especially for the power flowing back to the grid. If an LCL-filter is utilized, then there would be 6 inductors instead of one in the buck converter. As opposed to buck converters, rectifiers need 6 control signals whereas buck converters need only one or two.

The most usable option is to use the buck converter, the control strategy can be cascade or separately control for both, the output voltage and current. The control is simple since there is only one control signal and two required measurements, i.e. output voltage and current. If one IGBT is designed for continuous current of *300 A* [19] then two IGBTs need to be in parallel to achieve the rated maximum current *600 A*. An L-filter in the grid side should still be used for the current ratings are high for low-frequency harmonics.

The unknown price and high number of chargers exclude the battery chargers, leaving basically 2 options. However, the controllability of the active rectifier is limited or, rather the output of the transformer would be very low voltage, and the main benefit would be the bi-directional power flow which requires filtering and another control device before the battery modules. An inductor should be added to the grid side of the diode bridge if the grid current is desired to be kept sinusoidal. Controllability is much simpler with a DC-DC converter, even if the stress on the components is naturally greater in DC-DC converter for only one “phase” is in use, rather than 3 in the case of active rectifier. Furthermore, bi-directional power flow is difficult to implement, and the total efficiency is not an issue which recommend the use of buck converter.

The buck converter simulation model is discussed in 5. The cascade control and the separate controllers are compared to each other. In addition, the simulations are done with one large buck converter and with two smaller buck converters which should be synchronized perfectly to avoid problems. Two converters instead of one large converter would reduce the stress on the components and the size of the components. This would also reduce the high di/dt during changes in the reference, reducing noise radiated from the device and large components tend to have lower self-resonance frequency which can be avoided with smaller components [20]. Synchronization of the paralleled converters should be very accurate for the battery modules are series connected.

4. CONTROL OF BATTERY MODULE TESTER

Active switches of power converters need to be controlled. This chapter describes certain control aspects related to DC-DC converters, more accurately, to the buck converter which is used. The most used modulation method is pulse-width modulation (PWM) and in DC-DC converters it is based on duty ratio control. The control of the battery module tester is introduced in this chapter including system representation, transfer functions, feedback, PID-controller and PWM. The point behind control is to adjust current via a reference voltage.

4.1 System representation

Transfer functions and control theory related to implementation of the actual control system is discussed in this chapter. However, only the relevant issues in DC-DC converter perspective are discussed.

Modeling PWM switching converters requires an adequate model, for this purpose the state-space averaging method is used. The main idea of this method is to have a small-signal averaged model which requires the state equations of the converter and the system must be linearized. This small-signal model is an AC equivalent circuit of an DC-circuit and all nonlinear elements are substituted by linear elements to approximate the behavior of the variables near the selected steady-state. In other words, an unlinear system, such as buck converter, is linearized near an operating point to approximate the converter's behavior in its proximity. To develop this model, input variables, state variables and output variables must be derived. The state variables are expressed as linear combinations of the system independent inputs and the state variables themselves. The state variables are inductor currents and capacitor voltages in DC-DC applications. The input variables are the independent inputs to the system, for example usually the input voltage is known, and the load can be modeled either using a voltage source or a current source. The output variables can be calculated if the state variables and the input variables are known. [7], [11]

At the steady-state, the values are constant, and if the system is linear time-invariant (LTI) these relationships can be expressed as in Eq. 4.1 and in Eq. 4.2.

$$\dot{x} = Ax + Bu \tag{4.1}$$

$$y = Cx + Du \tag{4.2}$$

Where *x* is the state vector, *u* the input vector and *y* the output vector. A, B, C and D are the state, input, output and feed-through matrices [21]. The detailed process of the mathematical part is not in the scope of this thesis. However, the whole process is shown in appendixes A and B.

Dynamic systems are usually represented by transfer functions which are used to describe processes by mathematical equations. A DC-DC converter has 6 transfer functions [7] of which one is especially important, control-to-output transfer function assuming an output variable is the quantity which is controlled. It is used to gain knowledge what is the relationship between the output variable, for example voltage or current, and the duty ratio. This transfer function can be used for tuning the controller.

Transfer functions can be in different domains but in this thesis, all transfer functions are in Laplace -domain which are in complex plane. First, time-domain equations are converted, *s* in the transfer function [11] is replaced with *jω* thereafter the magnitude is calculated with the absolute value of a complex number. After the replacement the transfer function is in frequency domain. The phase is calculated by dividing *y* with *x*, where *x* is the real value and *y* the imaginary value. In a transfer function, zeros are the solutions for s when numerator is equal to zero and poles of the system are the solutions for s where nominator is equal to zero. A simple transfer function is shown as equation 4.3.

$$Y(s) = \frac{(Ms+b)}{(Ms^2+bs+k)} = \frac{p(s)}{q(s)} \tag{4.3}$$

The denominator polynomial *q(s)* equaling to zero is called the characteristic equation because the roots of this equation are responsible for the character of the *time response*. The roots of this characteristic equation are called poles of the system. The roots of the numerator polynomial *p(s)* are called as zeros of the system. [22]

It is necessary to understand stability to achieve a stable control system. Zeros and poles of a certain transfer function can be plotted, and y-axis is imaginary axis and x-axis is real axis in complex plane. Left-half plane (LHP) is defined as the negative axis of the real axis. All the poles need to be in the LHP for stable operation which means that the poles are negative in real axis. Right-half plane (RHP) zeros can be mitigated with certain requirements, but it is not in the scope of this thesis. Effects of RHP-pole and -zero are illustrated in Figure 14.

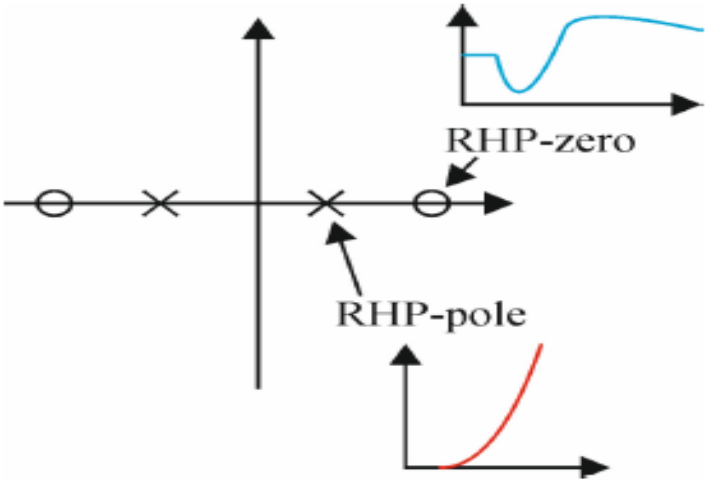

Figure 14. RHP zero and pole effects [23].

Zeros in the RHP cause step-response to opposite direction and poles in the right-half plane cause the system to become unstable as in Figure 14. LHP-zeros are used to increase the phase margin and poles are used to filter noise. The phase margin needs to be high enough, lack of phase margin will lead to overshoot during a step response. Crossover frequency should also be as high as possible. It is proportional to settling time. Thus, a small crossover frequency means longer settling time. The minimum gain margin is *6 dB* and the minimum value for stable phase margin is *45°*. Phase margin and gain margin will be discussed in chapter 5.2. [7], [23]

4.2 Feedback-control

Feedback-control is used in this study, to control the difference between the reference value and the measured value i.e. the control error [24]. The control error is fed to PID-controller, and the duty ratio is controlled, which is the on-time of the switch during one period. If an open-loop control would be used, the control would not be accurate or in the worst-case scenario it would lead to instability. An open-loop system and a closed-loop system are shown in Fig. 15.

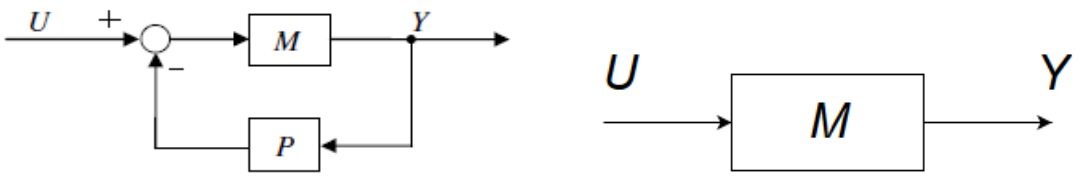

Figure 15. Closed-loop control on the left and open-loop control on the right.

In an open loop system in Fig. 15 the system operates without feedback, directly generating the output in response to an input signal. In contrast to the open-loop system, a closed-loop system uses a feedback which is measurement of the output signal and

compares it to a desired output reference to generate an error signal that is used by the controller. The output of the open-loop system is in Eq. 4.4.

$$Y = MU \tag{4.4}$$

Where U stands for the input signal, Y for the output signal and M and P are transfer functions. The closed-loop system has a bit more complicated output as shown in Eq. 4.5.

$$Y = M(U - PY) \tag{4.5}$$

As Eq. 4.5 is solved for Y, the resulting transfer function is visible in Eq. 4.6.

$$Y = \frac{M}{1+MP}U \tag{4.6}$$

The relationship between the output and the input is the corresponding transfer function for the system is shown in Eq. 4.7. Transfer functions can be thought as the relationship between an output variable and an input variable, or between a state variable and an output variable.

$$G = \frac{Y}{U} = \frac{M}{1+MP} \tag{4.7}$$

In practice, U could represent the reference output voltage while Y could be substituted with the actual, measured output voltage. M represents in this scenario the controller and P the measurement gain. This kind of controller is simple, and the reference voltage adjusts the actual output according to the gains M and P.

An example of closed-loop control is shown in Figure 16. The control error is connected to the compensator, which usually is a PI-controller. This controlled error v_c in Fig. 16 is in turn used as an input to the pulse-width modulator which is responsible for adjusting the on- and off-time of the switch.

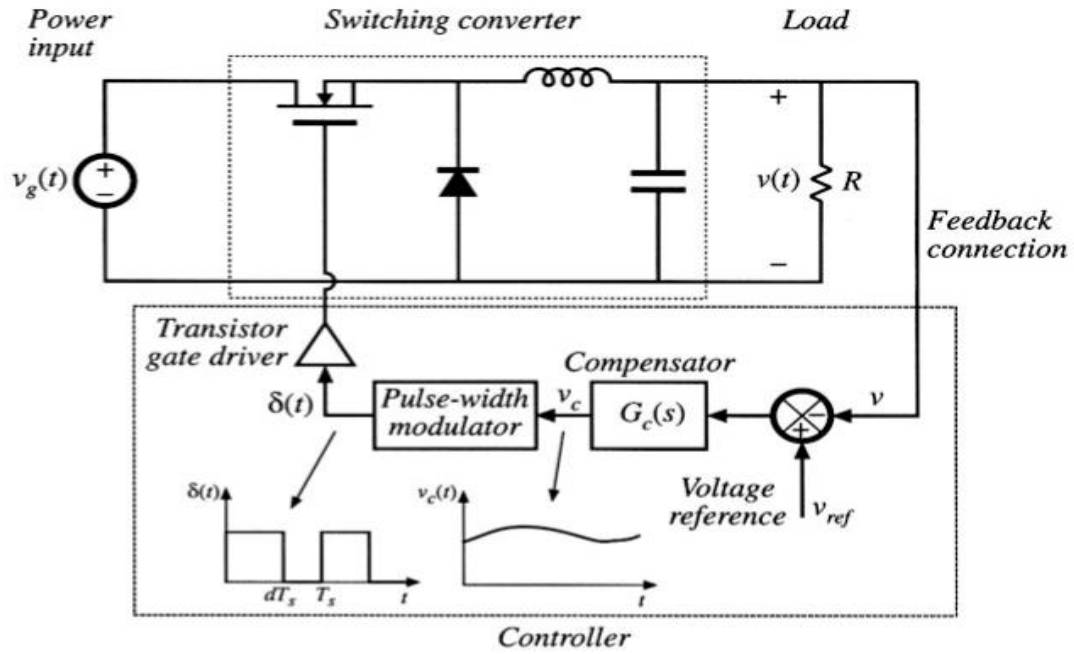

Figure 16. Feedback controlled buck converter [11].

The target of the feedback control is to minimize the difference between the desired and the actual value, even without an accurate model of the battery modules. The controller is responsible for adjusting the control error to zero. A feedback system using PID-controller illustrated in Figure 17 with practical transfer functions. A controller which uses only proportional control will have a steady state error (≠0) because some level of control is required to maintain a desired value [24], but usually PI-control can achieve satisfactory results. However, PID-controller can yield even better results. PI-controller is used in this thesis.

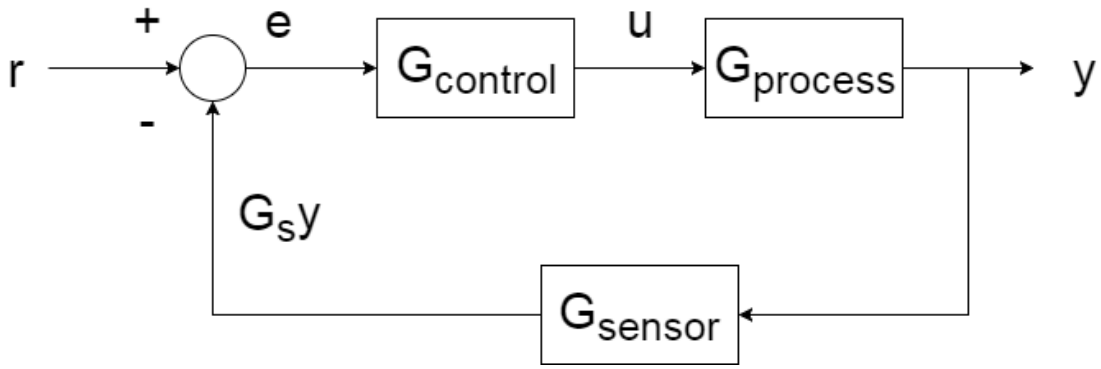

Figure 17. Block diagram of a control system.

The PLC will be in charge of the control of the battery module tester. The gain parameters can be adjusted either manually or automatically. It can be based on the trial and error -method or on simulations which is why loop gains are solved and tuned. This thesis provides control parameters for PI-controller which are shown in chapter 6.1.

4.3 Pulse-width modulation of DC-DC converters

Pulse-width modulation is crucial for adjusting on and off times of the switches in case of DC-DC converters. Many microcontrollers and digital signal processors (DSP) include on-chip PWM controllers. Pulse-width modulators are used for producing a logic signal that commands the converter power transistor to switch on or off. This signal is periodic, with certain frequency and duty ratio. The input signal is an analog control signal which is compared to a sawtooth wave signal by an analog comparator which is shown in Fig. 18. The analog input signal is the output *y* shown in Figure 17. The sawtooth wave signal is also called as the carrier signal. The frequency of the sawtooth waveform defines the switching frequency of the active switch in the DC/DC converter. [11], [22]

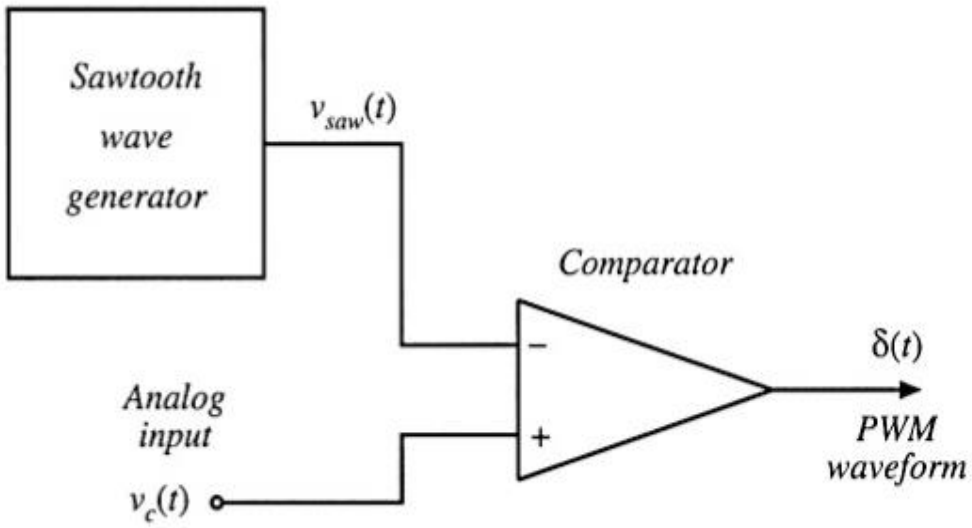

Figure 18. Analog signal is compared to sawtooth wave generator [11].

The output of this arrangement is shown in Figure 19. The peak-to-peak voltage of this sawtooth wave generator is V_M, and for the duty cycle to be linear the control input must be limited between 0 and V_M. The duty ratio would be *0 %* or *100 %*, if the control input was not limited.

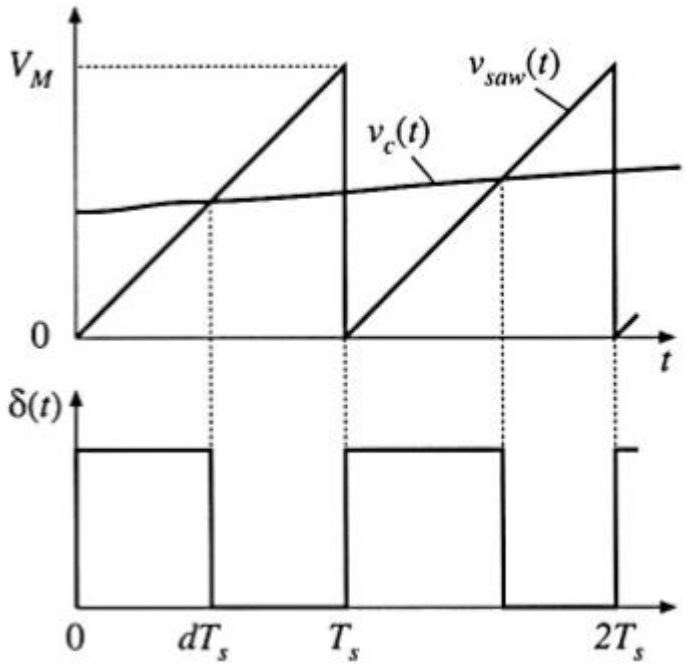

Figure 19. PWM for DC-DC converters [11].

The carrier signal state is linear from *0 V* up to V_M within one switching period and repeating the same pattern after finishing the period. The control signal is compared to this sawtooth wave signal and every time the control signal is greater than the carrier signal, the comparator output is equal to the supply voltage. Otherwise, the output will be equal to ground potential *0 V*. The amplitude of the output is fixed, and the maximum duty cycle is usually limited to *95 %* depending on the converter topology. [25]

5. BUCK ANALYSIS

The buck converter was chosen to be used for controlling the battery modules. To tune the controller, all parameters, such as capacitor, inductor, equivalent series resistances (ESR), switching frequency, should be known. The switching frequency is selected to be *5 kHz* to guarantee that the required current can be delivered by the IGBTs [19]. The high current limits the switching frequency.

First, the required capacitance and inductance values are dimensioned after which the control design is discussed. Voltage mode -control and current mode -control are applied in the controller. This means that the output voltage is first compared to its reference value and after surpassing this value, the control changes to the current control in which the reference is a current reference which is compared to the measured current. The voltage mode -control is applied until the current has reached its setpoint after which the current reference is utilized. In other words, the target is to adjust voltage first and as the duty ratio of the switches increases, the current will increase. The control is switched to current mode -control when the reference current is surpassed. Even if the separate control method uses current and voltage controllers, the primary target is to control the current flowing to the battery modules. In a way this control strategy protects from overcurrent. This is the idea for separate controllers, for the cascade control the control strategy is discussed in its own chapter 5.3. Simulations are done using separate controllers for one large buck converter and for two smaller buck converters in parallel and the last simulation uses cascade control in one buck converter.

5.1 Component selection

Some components are already available at the workplace, including IGBT modules, diode bridge, fuses, diodes, cables, PLC units and switching devices. The IGBT modules include their own drivers and are rated up to *1200 V* in terms of collector-to-emitter voltage. All components are dimensioned to withstand the current and voltage limits. Only the passive components need to be chosen.

According to the inductor volt-second balance or, rather, the average inductor-voltage over one period must be zero [7]. During on-time, voltage over inductor is equal to U_{in} - U_o while at off-times the voltage is $-U_o$, if ESRs are neglected.

$$\int_0^{DT_s} u_{L,on}dt + \int_{DT_s}^{T_s} u_{L,off}dt = 0$$

$$\int_0^{DT_s} U_{in} - U_o dt + \int_{DT_s}^{T_s} (-U_o) dt = 0$$

$$DT_s U_{in} - DT_s U_o + T_s(-U_o) - DT_s(-U_o) = 0$$

$$M(D) = \frac{U_o}{U_{in}} = D \tag{5.1}$$

Where U_o is the output voltage, U_{in} the input voltage and D the duty ratio at steady state. Eq. 5.1 means that the duty ratio D is equal to the ratio of output voltage and input voltage which, in general, should be the relationship. As D is known, other parameters are known to solve a suitable inductor size as follows in Eq. 5.2.

$$v_L = L \frac{di_{L-pp}}{dt} \tag{5.2}$$

Where v_L is the inductor voltage, L the inductor value and $\Delta i_{L\text{-}pp}$ stands for the peak-to-peak inductor current ripple. The inductor size can be solved either using on- or off-time as shown below in Eq. 5.3 and 5.4.

$$v_{L,on} = L \frac{\Delta i_{L-pp}}{DT_s} \tag{5.3}$$

$$v_{L,off} = L \frac{\Delta i_{L-pp}}{(1-D)T_s} \tag{5.4}$$

Where T_s is the period, other parameters were defined above. The final equation for solving L is Eq. 5.5 which is solved by putting the above equation on-time inductor voltage 5.3 to equation 5.2. Eq. 5.6 is the same as Eq. 5.5, only the solved quantity is changed.

$$L = \frac{DT_s(V_{in}-V_o)}{\Delta i_{l-pp}} \tag{5.5}$$

$$\Delta i_{l-pp} = \frac{DT_s(V_{in}-V_o)}{L} \tag{5.6}$$

Differentiating Eq. 5.6 with respect to V_o and solving the derivative yields Eq. 5.7.

$$\Delta i_{l-pp} = \frac{V_{in} - V_o}{L} \frac{V_o}{V_{in}} T_s = \frac{V_o T_s}{L} - \frac{T_s {V_o}^2}{V_{in} L}$$

$$\frac{\Delta i_{l-pp}}{dV_o} = \frac{T_s}{L} - \frac{2T_s V_o}{V_{in} L}$$

$$\frac{T_s}{L} - \frac{2T_s V_o}{V_{in} L} = 0$$

$$V_o = \frac{1}{2} V_{in} \tag{5.7}$$

At this point the current ripple is at its maximum. Since the current range is *60-600 A*, the minimum value for *D* is when current equals to *60 A*. The resulting duty ratio is:

$$D = \frac{(50\ \text{m}\Omega + 10\ \text{m}\Omega) \cdot 60\ \text{A} + 120\ \text{V} + 2\ \text{V}}{170\ \text{V} - (1\ \text{m}\Omega - 10\ \text{m}\Omega) \cdot 60\ \text{A} + 2\ \text{V}}$$

$$D = 0.7279$$

L size can be calculated by Eq. 5.5. The allowable ripple is assumed to be *10 %*.

$$L = \frac{170\ V - 120\ V}{60\ A \cdot 10\ \%} \cdot 0.7279 \cdot \frac{1}{5\ kHz}$$

$$L = 1.2\ mH$$

If the current ripple would be *5 %*, the inductor size would be *2.4 mH*. However, *1.2 mH* is adequate in this application since it guarantees small ripple and it is smaller and cheaper compared to an inductor which is *2.4 mH*. This inductor is shown in Figure 6 as the inductor of the buck converter. The current ripple in the situation of the maximum charging current *600 A* is:

$$\Delta i_{l-pp} = \frac{170\ V - 120\ V}{1.2\ mH} \cdot 0.89 \cdot \frac{1}{5\ kHz} = 7.4\ A$$

The inductor should not saturate under the maximum load current, otherwise it is not usable. Furthermore, a low value for ESR is desired to avoid induced voltage drops [26].

Inductors tend suffer a reduction in inductance as current increases, eventually up to a point where the inductor has no inductance at all. This is the saturation of an inductor. In EMI-perspective, the best alternative is to use an inductor which has a closed magnetic circuit [27], such as toroids. If an inductor with an air gap is used stray fields will be larger, but the saturation does not happen so easily.

Ferrites could be used for low-pass filtering [26], since at high frequencies ferrites become resistive and can filter the high frequency components of the signal. At low frequencies ferrites behave similarly compared to inductors. Ferrites can be understood as inductors at low frequencies and as a combination of a resistor and an inductor at high frequencies. There are manufacturers who produce round-cable ferrites, such as [28], but the current ratings are not available.

Capacitors have different operating frequencies depending on the type of the capacitor. If required operating frequency is in the range of kilohertz, aluminium electrolytic ca-

pacitors are a good choice since these capacitors can be used in a wide range of voltage rates and sizes. The voltage range is up to *500 V* and one of their qualities is a high capacitance-to-volume ratio. A minor drawback is that they are polarized, i.e. cannot tolerate reverse voltages. Considering their operation, capacitors have equivalent series resistance (ESR) as well as equivalent series inductance (ESL) which means no capacitor is purely capacitive. [29]

As was mentioned ESR is one of capacitors' parameter. The larger size a capacitor has, the smaller is the ESR value of the capacitor. So, to give some perspective, an aluminium capacitor, which has a size of *100 μF*, has ESR value of *377 m*Ω. In comparison a capacitor of *1200 μF* has ESR value of only *75 m*Ω [30]. The capacitor size is determined by Eq. 5.8. In this the voltage ripple can be *5 %*.

$$\Delta v = \frac{\Delta i_L T_s}{8C}$$

$$C = \frac{\Delta i_L T_s}{8\Delta v} \tag{5.8}$$

$$C = \frac{60\ A \cdot 10\ \% \cdot \frac{1}{5000\ Hz}}{8 \cdot 5\ \% \cdot 120\ V}$$

$$C = 0.000025\ F = 25\ \mu F$$

If, however, the maximum current ripple is chosen, i.e. the ripple when batteries are charged with current of *600 A*, the capacitor size is:

$$C = \frac{7.4\ A \cdot \frac{1}{5000\ Hz}}{8 \cdot 5\ \% \cdot 120\ V} = 31\ \mu F$$

With *2 %* voltage ripple:

$$C = \frac{7.4\ A \cdot \frac{1}{5000\ Hz}}{8 \cdot 2\ \% \cdot 120\ V} = 77\ \mu F$$

With some safety margin an electrolytic capacitor of *100 μF* is chosen for the output capacitor since the frequency is low. The ESL of the capacitors should be low to avoid self-resonance. Furthermore, the voltage rating should be high enough to match the requirements set by the output current and voltage.

The input capacitor value can be determined by simulating or by calculating. In this case, simulating is utilized and below are illustrated waveforms with following capacitances: *100 μF* and *0.01 F* (Figure 20 and Figure 21). In these simulations a buck con-

verter is used, and the circuit is shown in Figure 1, and the load current is adjusted to *300 A*. The idea is to dimension the capacitor before the buck converter in Figure 6.

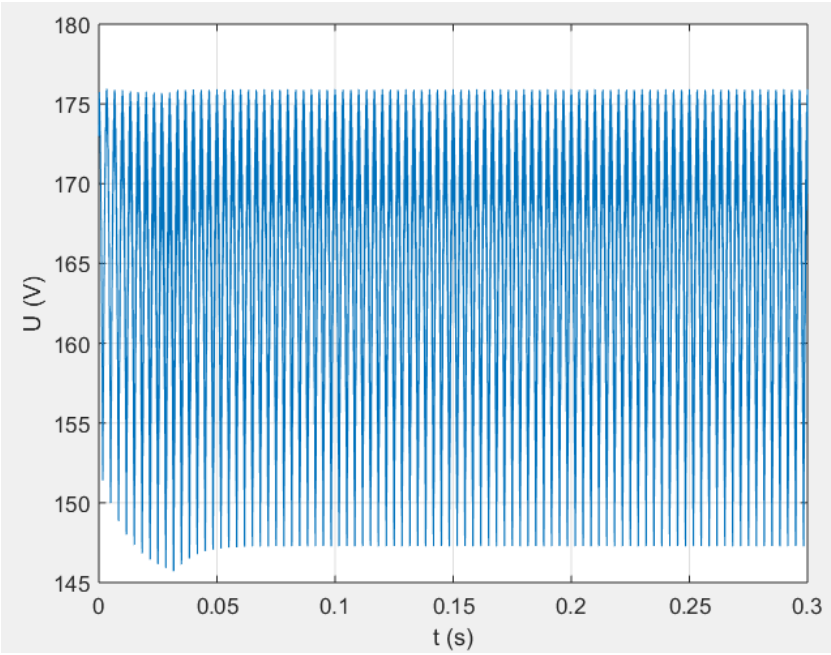

Figure 20. Input voltage ripple, C = 100 µF and R_c = 0.377 Ω.

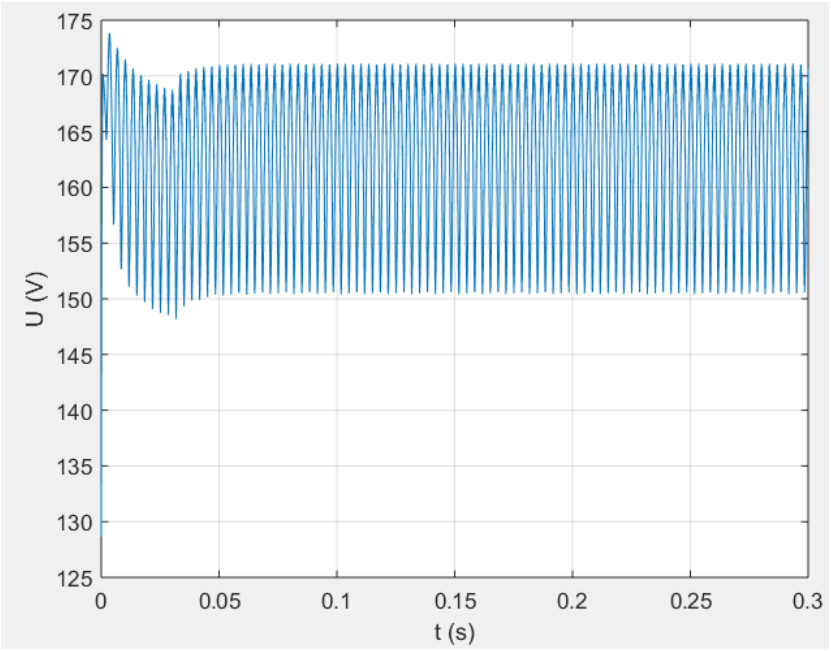

Figure 21. Input voltage ripple, C = 0.01 F and R_c = 0.004 Ω.

Based on the simulations, it seems that to reduce the ripple, the input capacitor must be at least millimetre farads. The *100 µF* input capacitor provides a ripple voltage of almost *30 V*, while the *10 mF* capacitor decreases the peak-to-peak ripple to *19 V*. However, with accurate control the input voltage ripple is not that important. The input capacitor can be larger to avoid ripple and improve quality of the load current, but it

should have a pre-load circuit to avoid high start transient current. In this case a capacitor of *1 mF* could be used.

All component values are known and are shown in Table 1. Some of the parameters are estimated values, but others are known values and taken from the datasheets which are shown in references. The battery estimated impedance *4 mΩ* is given for one battery and the total impedance for *5* batteries in series is equal to *20 mΩ*.

Table 1. Initial buck parameters.

Inductor size, L	*1.2 mH*	Diode voltage, V_d	*2 V*
Equivalent series resistance, r_L	*50 mΩ*	Input voltage, V_{in}	*170 V*
Capacitance, C	*100 μF*	Output voltage, V_o	*120 V*
Equivalent series resistance, r_C	*20 mΩ*	Output current, I_o	*50 - 600 A*
Switch resistance, r_{sw}	*1mΩ*	Switching frequency, f_s	*5 kHz*
Diode resistance, r_d	*10 mΩ*	Period, T_s	*0.2 ms*
Battery impedance, r_s	*4 mΩ*	Total battery impedance, $r_{s\text{-}tot}$	*20 mΩ*

Simulations are done tuning controllers for output current of *300 A*, and the total open circuit of voltage of 5 batteries in series is assumed to be *120 V* or *24 V·5*. The equivalent series resistances r_C and r_L are directional values, not necessary the exact values. The input voltage is *170 V* to gain allowable duty ratios, otherwise the switch would be *100 %* closed for some periods.

5.2 Separate controller

This section is divided into two chapters because of the nature of the controller. In the first case, 5.2.1, it is assumed that the input voltage and the output current are known. The output voltage can be controlled by assuming constant current which is chosen to be *300 A*, responding half of the maximum discharging/charging current.

The second chapter, 5.2.2, is about controlling the output current. To do this, the input voltage and the output voltage are assumed to be known. The output voltage is chosen to be *120 V* which is the rated value for 5 battery modules in series. The resulting control-to-output transfer functions are equal for both the separate controller and the cascade control, but the loop gains are not.

5.2.1 Voltage-fed voltage-output mode

In VFVO, the input variables, i.e. the known variables, are the input voltage and the output current. The on- and off-time equations are first solved. Average state space is in a nutshell a way to form an average value of on- and off-time equations. These values can be used to solve steady-state values and linearize the equations. The linearized equations are shown in appendix A for space saving.

In simulation perspective, it is needed to know what the control-to-output transfer function is. In Eq. 5.9 *G(s)* is the transfer function from input-to-output and it is shown also in Eq. 5.10.

$$Y(s) = G(s)U(s) \tag{5.9}$$

This Eq. 5.10 is equal to VF/VO G-parameters in Eq. 5.10. These transfer functions are open loop transfer functions.

$$\begin{bmatrix} \hat{\imath}_{in} \\ \hat{v}_o \end{bmatrix} = \begin{bmatrix} {Y_{in}}^G & {T_{oi}}^G & {G_{ci}}^G \\ {G_{io}}^G & -{Z_o}^G & {G_{co}}^G \end{bmatrix} \begin{bmatrix} \hat{v}_{in} \\ \hat{\imath}_o \\ \hat{c} \end{bmatrix} \tag{5.10}$$

The output variables are the input current and the output voltage as in Eq. 5.10 and $\hat{c}$ denotes to the control variable which in case of converters is usually the duty ratio. This is the last step of linearization. The transfer function G_{co}, i.e. control-to-output, is used for tuning the controller. The linearized state space for the output and state variables are shown below. These equations are used to form matrices as explained in chapter 4. Linearization is obtained by using partial derivatives for state, input and output variables. Subscript '^' denotes to a linearized variable. The diode forward voltage drop v_d is not a variable, but rather assumed to be constant so it is not differentiated. The linearized state space is presented in Eq. 5.11 – 5.17.

$$\frac{d\hat{\imath}_L}{dt} = \frac{1}{L}\left(D\hat{v}_{in} - R_1\hat{\imath}_L - \hat{v}_{c_{out}} + r_{C_{out}}\hat{\imath}_o + R_2\hat{d}\right) \tag{5.11}$$

$$\frac{d\hat{v}_{c_{in}}}{dt} = \frac{1}{r_{c_{in}}C_{in}}\hat{v}_{in} - \frac{1}{r_{c_{in}}C_{in}}\hat{v}_{c_{in}} \tag{5.12}$$

$$\frac{d\hat{v}_{c_{out}}}{dt} = \frac{1}{C_{out}}(\hat{\imath}_L - \hat{\imath}_o) \tag{5.13}$$

$$\hat{\imath}_{in} = D\hat{\imath}_L + \frac{1}{r_{c_{in}}}\hat{v}_{in} - \frac{1}{r_{c_{in}}}\hat{v}_{C_{in}} + I_L\hat{d} \tag{5.14}$$

$$\hat{v}_o = \hat{v}_{C_{out}} + r_{C_{out}} \cdot (\hat{\imath}_L - \hat{\imath}_o) \tag{5.15}$$

In which:

$$R_1 = Dr_{sw} + r_L + r_{C_{out}} + D'r_d \tag{5.16}$$

$$R_2 = V_{in} - r_{sw}I_o + r_dI_o + v_d \tag{5.17}$$

All the factors in Eq. 5.11-5.15 are inserted into matrices ***A***, ***B***, ***C*** and ***D*** according to the input variables shown in Eq. 5.18 and in Eq. 5.19. The state variables are located to the left side of Eq. 5.18 and the output variables in Eq. 5.19. Both are solved from the state variables and the input variables. For example, in the first row and column of ***A*** in Eq. 5.18 the factor is $-R_1/L$ because this is the coefficient solved in Eq. 5.11.

$$\frac{d}{dt}\begin{bmatrix} \hat{\imath}_L \\ \hat{v}_{C_{in}} \\ \hat{v}_{C_{out}} \end{bmatrix} = \overbrace{\begin{bmatrix} -\frac{R_1}{L} & 0 & -\frac{1}{L} \\ 0 & -\frac{1}{r_{c_{in}}C_{in}} & 0 \\ \frac{1}{C_{out}} & 0 & 0 \end{bmatrix}}^{\boldsymbol{A}} \begin{bmatrix} \hat{\imath}_L \\ \hat{v}_{C_{in}} \\ \hat{v}_{C_{out}} \end{bmatrix} + \overbrace{\begin{bmatrix} \frac{D}{L} & \frac{r_{c_{out}}}{L} & \frac{R_2}{L} \\ \frac{1}{r_{c_{in}}C_{in}} & 0 & 0 \\ 0 & -\frac{1}{C_{out}} & 0 \end{bmatrix}}^{\boldsymbol{B}} \begin{bmatrix} \hat{v}_{in} \\ \hat{\imath}_o \\ \hat{d} \end{bmatrix} \tag{5.18}$$

$$\begin{bmatrix} \hat{\imath}_{in} \\ \hat{v}_o \end{bmatrix} = \overbrace{\begin{bmatrix} D & -\frac{1}{r_{c_{in}}} & 0 \\ r_{C_{out}} & 0 & 1 \end{bmatrix}}^{\boldsymbol{C}} \begin{bmatrix} \hat{\imath}_L \\ \hat{v}_{C_{in}} \\ \hat{v}_{C_{out}} \end{bmatrix} + \overbrace{\begin{bmatrix} \frac{1}{r_{c_{in}}} & 0 & I_o \\ 0 & -r_{C_{out}} & 0 \end{bmatrix}}^{\boldsymbol{D}} \begin{bmatrix} \hat{v}_{in} \\ \hat{\imath}_o \\ \hat{d} \end{bmatrix} \tag{5.19}$$

Eq. 5.18 and Eq. 5.19 corresponds to earlier shown equations 3.1 and 3.2 which are shown here for convenience as Eq. 5.20 and Eq. 5.21.

$$\dot{x} = Ax + Bu \tag{5.20}$$

$$y = Cx + Du \tag{5.21}$$

The actual transfer functions can be solved by Eq. 5.20 and Eq. 5.21 which is shown in Eq. 5.22.

$$\boldsymbol{G} = \boldsymbol{C} \cdot (s \cdot \boldsymbol{I} - \boldsymbol{A})^{-1} + \boldsymbol{D} \tag{5.22}$$

Where ***I*** is the identity matrix and ***G*** the transfer functions. The last step before simulation is to solve the control-to-output transfer function which is done in MATLAB. This transfer function presents the relationship between the control variable and the output variable. The control-to-output transfer function is also solved taking the load effect (battery impedance) into account which is shown in Eq. 5.23.

$${G_{co}}^{L-G} = \frac{{G_{co_o}}^{G}}{1+\frac{{Z_o}^{G}}{Z_L}} \tag{5.23}$$

Where ${G_{co_o}}^{G}$ is the open-loop control-to-output transfer function, ${Z_o}^{G}$ is the open-loop output impedance, Z_L is the load impedance which is the battery and ${G_{co}}^{L-G}$ is the load

affected control-to-output transfer function. ^{G} denotes to the input variables. In Eq. 5.23 the open loop transfer functions $G_{co\text{-}o}$ and $Z_{o\text{-}o}$ are needed for solving the actual load affected transfer function.

The load effect is demonstrated with a bode plot shown in Figure 22. Bode plots or diagrams show magnitude and phase of a transfer function in frequency domain. Magnitude is in decibels and phase in degrees. Important issues are crossover frequency, phase margin and gain margin. The gain margin is defined to be the factor by which the gain factor K can be multiplied before the closed-loop system becomes unstable. The definition of the phase margin is the amount of additional open-loop phase shift required at unity gain to make the closed-loop system unstable. The crossover frequency is the frequency when the magnitude of the loop gain is unity which in decibels is equal to $0\ dB$. The phase margin is the phase at the crossover frequency $+180°$. Stability of the system can be assessed with the phase margin test. [11]

The tuning of the controller can be done using either of the control-to-output transfer functions, but in this case, it is done based on the load affected transfer function $G_{co}^{\ L-G}$ to yield more accurate result.

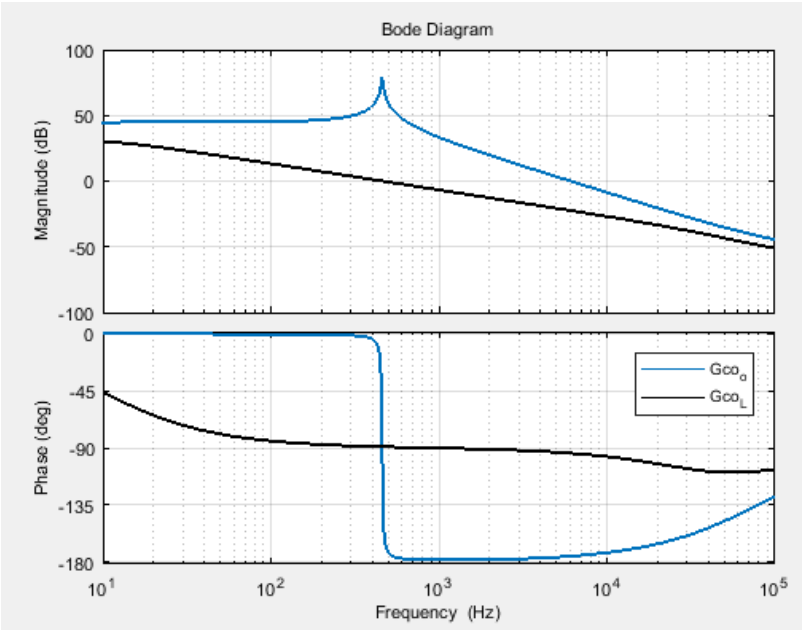

Figure 22. Control-to-output transfer functions with and without the load effect.

The load effect has a significant effect on both, phase and magnitude. The load effect in $G_{co\text{-}L}$ has eliminated LC –resonance which is visible in the other transfer function without the load effect, $G_{co\text{-}o}$. The load affected transfer functions are used in tuning PI-controllers.

The next step is to tune the controller having a sufficient gain and phase margin. This is done using a simple PI-controller. Controller zeros are used for increasing phase margin

and poles are used to reduce gain in frequencies of no interest. The same thing is done for the current transfer functions later in chapter 5.2.2.

There are some constraints for PI-controller tuning in power electronics. First, the crossover frequency should be limited to 1/5 of the switching frequency, where f_s is the switching frequency for avoiding the switching frequency ripple and possible instability. Sufficient margins are 45 degrees for phase margin and *6 dB* for gain margin for stable system. Unstable system has a crossover frequency with a phase margin of 0^o and a gain margin of *0 dB*. If there was an RHP-zero, then the crossover frequency should be less than the RHP-zero. If an RHP-pole existed, then the crossover frequency should be higher than the frequency of the RHP-pole. In this case there are no RHP-poles or -zeros, so the limiting factor for the crossover frequency is only the switching frequency. The tuned voltage loop gain is shown in Figure 23 and the controller transfer function in Eq. 5.24. [7]

$$K_{dc} = 10^{50/20}$$

$$\omega_{z1} = 40 \cdot \pi$$

$$\omega_{p1} = \frac{5000}{1.8} \cdot \pi$$

$$G_{cv} = K_{dc} \frac{\left(1+\frac{s}{\omega_{z1}}\right)}{\left(1+\frac{s}{\omega_{p1}}\right)} \tag{5.24}$$

Where G_{cv} is the controller transfer function for the voltage loop, K_{dc} is the DC gain, ω_{z1} and ω_{p1} are the crossover frequencies for the zero and the pole of the controller. The loop gains consider the control-to-output transfer function and the controller transfer function. In real systems, measurement gain must be also considered, but in this the measurement gain is simply 1. This can be scaled in a digital controller, such as PLC. The loop gains for the load affected control-to-output transfer function and the open-loop control-to-output transfer functions are shown in bode plot in Fig. 23.

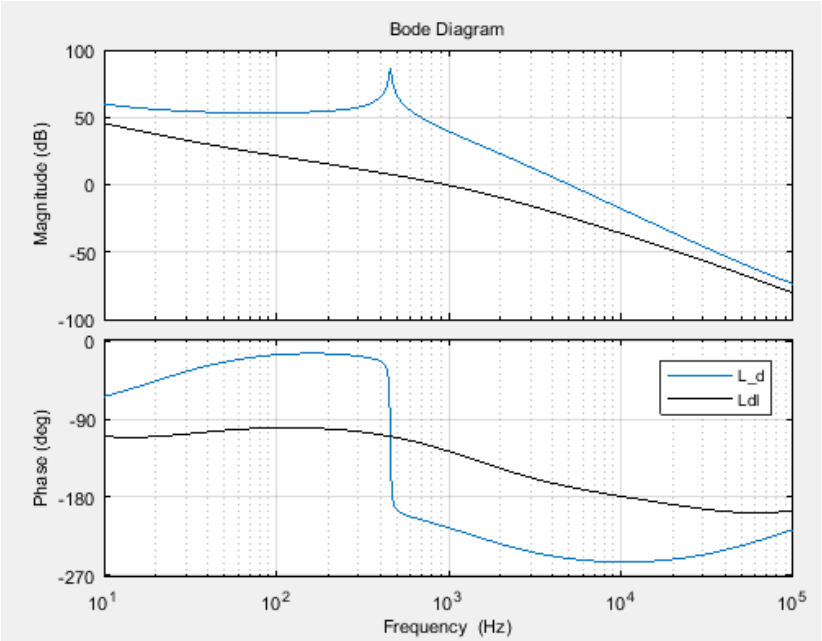

Figure 23. Loop gain for G_{co} functions.

The phase margin for the load affected transfer function is *54.1°* and the gain margin is *37.2 dB*. The phase margin is the phase at the crossover frequency, i.e. magnitude equal to *0 dB* and the gain margin is the gain when the phase is *-180°*. The crossover frequency is tuned to roughly *1 kHz* which corresponds to 1/5 of the switching frequency.

5.2.2 Voltage-fed current-output mode

The same procedure is carried out for VFCO-mode, except the output current is controlled. VFCO-mode is voltage-fed current output mode, i.e. current is controlled, kept constant. Earlier, the input voltage and the output current were assumed to be known; now the input voltage and the output voltage are known which changes the dynamics of the converter. The VFCO Y –parameters are shown in Eq. 5.25.

$$\begin{bmatrix} \hat{\imath}_{in} \\ \hat{\imath}_o \end{bmatrix} = \begin{bmatrix} {Y_{in}}^Y & {T_{oi}}^Y & {G_{ci}}^Y \\ {G_{io}}^Y & -{Y_o}^Y & {G_{co}}^Y \end{bmatrix} \begin{bmatrix} \hat{v}_{in} \\ \hat{v}_o \\ \hat{c} \end{bmatrix} \tag{5.25}$$

The goal is to solve the control-to-output transfer function. Only equations which include the output voltage are replaced. The linearized state space is shown below in Eq. 5.26 – 5.32.

$$\frac{d\hat{\imath}_L}{dt} = \frac{1}{L}\left(D\hat{v}_{in} - R_3\hat{\imath}_L - \hat{v}_o + R_4\hat{d}\right) \tag{5.26}$$

$$\frac{d\hat{v}_{c_{in}}}{dt} = \frac{1}{r_{c_{in}}C_{in}}\hat{v}_{in} - \frac{1}{r_{c_{in}}C_{in}}\hat{v}_{c_{in}} \tag{5.27}$$

$$\frac{d\hat{v}_{c_{out}}}{dt} = \frac{1}{r_{c_{out}}C_{out}}\hat{v}_o - \frac{1}{r_{c_{out}}C_{out}}\hat{v}_{C_{out}} \tag{5.28}$$

$$\hat{\imath}_{in} = D\hat{\imath}_L + \frac{1}{r_{c_{in}}}\hat{v}_{in} - \frac{1}{r_{c_{in}}}\hat{v}_{C_{in}} + I_L\hat{d} \tag{5.29}$$

$$\hat{\imath}_o = \hat{\imath}_L - \frac{1}{r_{C_{out}}}\hat{v}_o + \frac{1}{r_{C_{out}}}\hat{v}_{C_{out}} \tag{5.30}$$

In which

$$R_3 = Dr_{sw} + r_L + D'r_d \tag{5.31}$$

$$R_4 = V_{in} - r_{sw}I_o + r_dI_o + v_d \tag{5.32}$$

Matrices ***A***, ***B***, ***C*** and ***D*** are solved similarly as in Eq. 5.18 and Eq. 5.19. The difference between these two, i.e. VFVO and VFCO, is that the input variables are different which alters these coefficients as well. The solved matrices are in Eq. 5.33 and in Eq. 5.34.

$$\frac{d}{dt}\begin{bmatrix}\hat{\imath}_L\\ \hat{v}_{C_{in}}\\ \hat{v}_{C_{out}}\end{bmatrix} = \overbrace{\begin{bmatrix}-\frac{R_3}{L} & 0 & -\frac{1}{L}\\ 0 & -\frac{1}{r_{c_{in}}C_{in}} & 0\\ 0 & 0 & -\frac{1}{r_{c_{out}}C_{out}}\end{bmatrix}}^{\boldsymbol{A}}\begin{bmatrix}\hat{\imath}_L\\ \hat{v}_{C_{in}}\\ \hat{v}_{C_{out}}\end{bmatrix} + \overbrace{\begin{bmatrix}\frac{D}{L} & -\frac{1}{L} & \frac{R_4}{L}\\ \frac{1}{r_{c_{in}}C_{in}} & 0 & 0\\ 0 & \frac{1}{r_{c_{out}}C_{out}} & 0\end{bmatrix}}^{\boldsymbol{B}}\begin{bmatrix}\hat{v}_{in}\\ \hat{v}_o\\ \hat{d}\end{bmatrix} \tag{5.33}$$

$$\begin{bmatrix}\hat{\imath}_{in}\\ \hat{v}_o\end{bmatrix} = \overbrace{\begin{bmatrix}D & -\frac{1}{r_{c_{in}}} & 0\\ 1 & 0 & \frac{1}{r_{C_{out}}}\end{bmatrix}}^{\boldsymbol{C}}\begin{bmatrix}\hat{\imath}_L\\ \hat{v}_{C_{in}}\\ \hat{v}_{C_{out}}\end{bmatrix} + \overbrace{\begin{bmatrix}\frac{1}{r_{c_{in}}} & 0 & I_o\\ 0 & -\frac{1}{r_{C_{out}}} & 0\end{bmatrix}}^{\boldsymbol{D}}\begin{bmatrix}\hat{v}_{in}\\ \hat{v}_o\\ \hat{d}\end{bmatrix} \tag{5.34}$$

The control-to-output transfer functions are plotted for VFCO-mode in Figure 24 and the tuned loop gain in Figure 25. The difference between the loop gains is not large as in Figure 23.

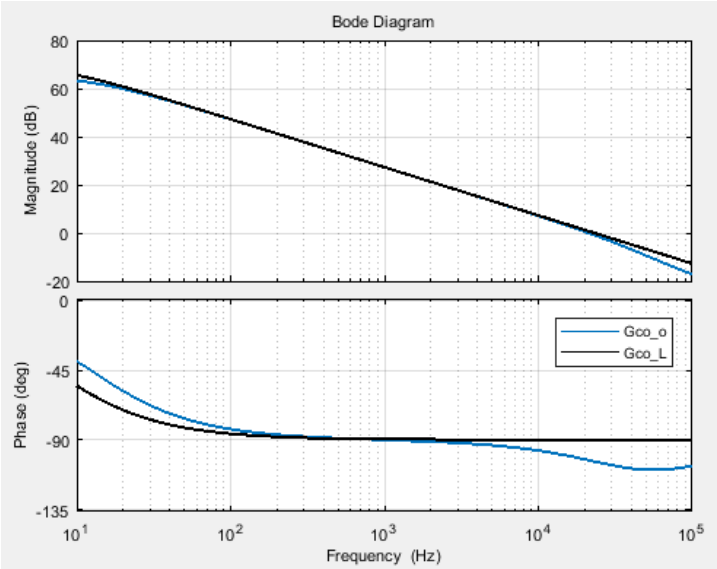

Figure 24. Control-to-output transfer functions.

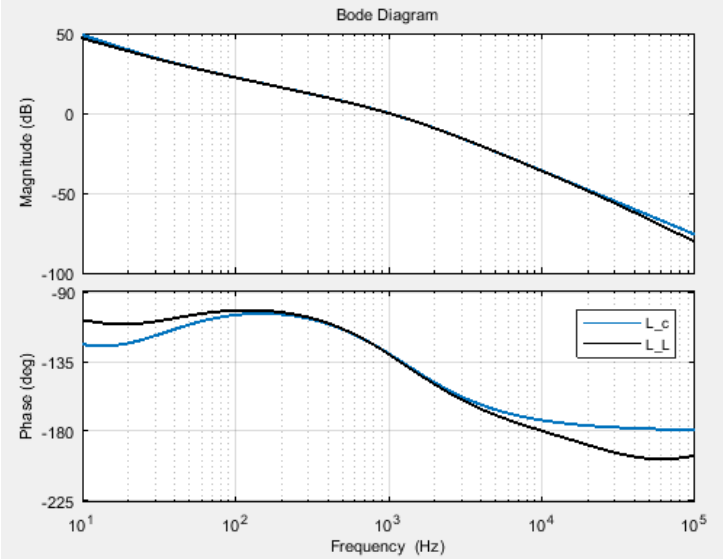

Figure 25. Loop gains.

The load effect has not as much effect on the loop gain as it had in the VFVO-case, but still the load affected transfer function is used in tuning. The tuning is done to have the crossover frequency of roughly *1 kHz*. The PM is *50°* and the GM is *40 dB*.

The first simulation is done with two buck converters in parallel shown in Figure 26 and for one large converter. Only the inductor value is decreased to be *75 %* of the dimensioned value for both converters, thus the total inductor value is *150 %* of the calculated value, *1.2 mH*. The dynamics are assumed to be the same and the PI-controllers are kept the same. Two similar converters instead of one has a lot of advantages including reliability, thermal management and converter stability [31]. It should be noted that there cannot be a significant delay between the two converters otherwise the operation will be inaccurate.

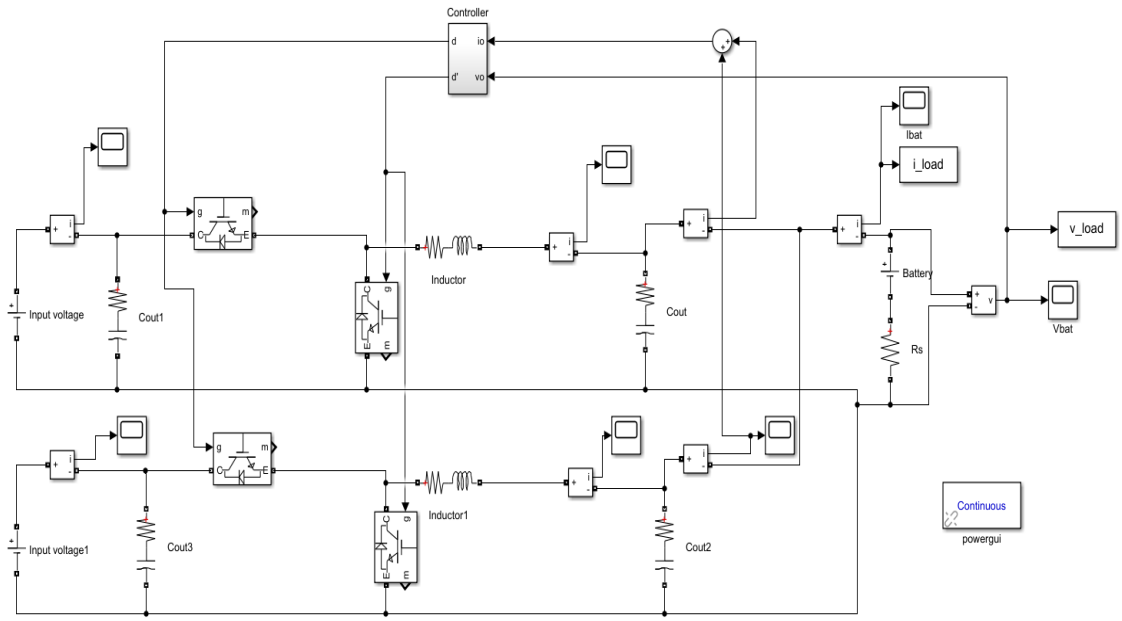

Figure 26. Schematics for two buck converters in parallel.

The simulations are done using a step change from *150 A* up to *300 A*. The current for both converters are shown in Fig. 27. The current waveforms are similar between the converters which should be the case in an ideal case. The stress on the components is halved which is reasonable with such high current levels.

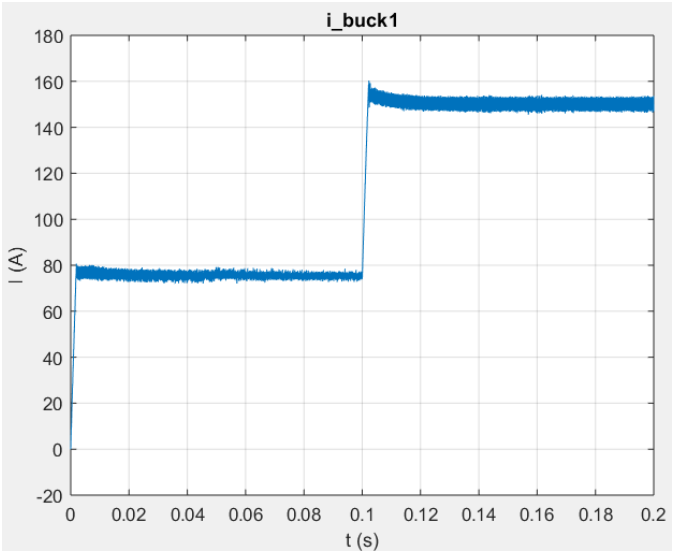

Figure 27. Current flowing through one converter.

The total current to the battery modules is shown in Fig. 28 and the total voltage over the battery series combination in Fig. 29. The total current corresponds to the sum of the currents flowing through each converter while the output voltage of the converters is similar.

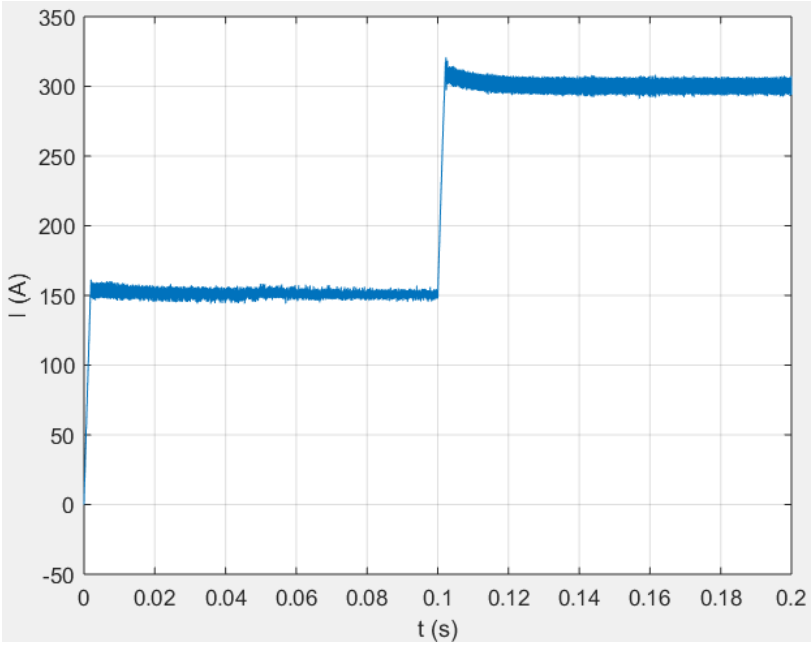

Figure 28. Total current.

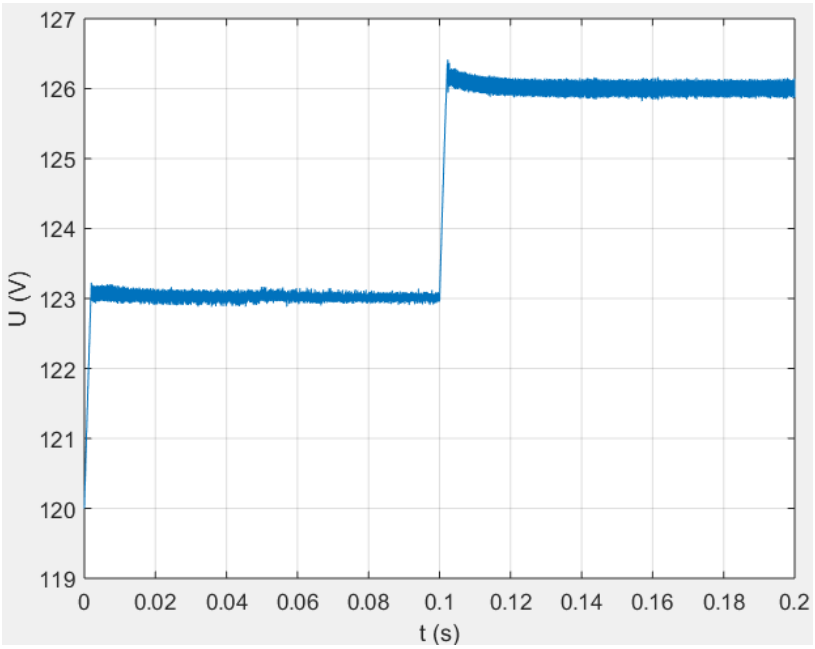

Figure 29. Battery voltage.

The voltage peak-to-peak ripple is around *0.3 V* at the steady state, when the transient is over at *0.1 s*. The current peak-to-peak ripple in Fig. 28 is *12 A*. However, the battery voltage cannot change that rapidly, which would lower the peak-to-peak ripples in all simulations presented in this thesis. The settling time, the time for the value to flatten in *+/- 5 %* of the reference value, is only *2 ms*, while the overshoot is *13 %* of the *150 A* step.

One big buck converter is simulated and the measured output current and voltage are shown in Fig. 30 and in Fig. 31. The stress on the components is much larger in this

case than in the two-converter topology. The step change is done similarly compared to the earlier case.

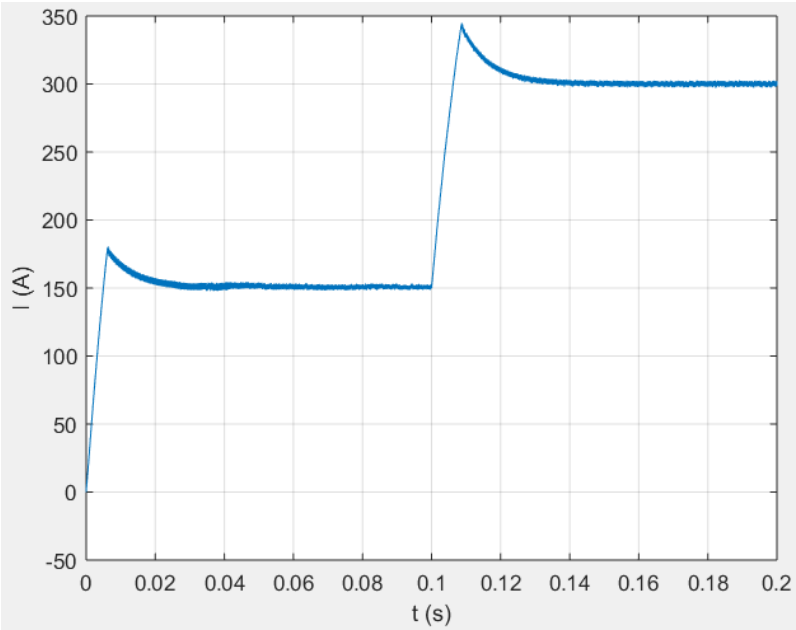

Figure 30. Current using one big buck converter during step response.

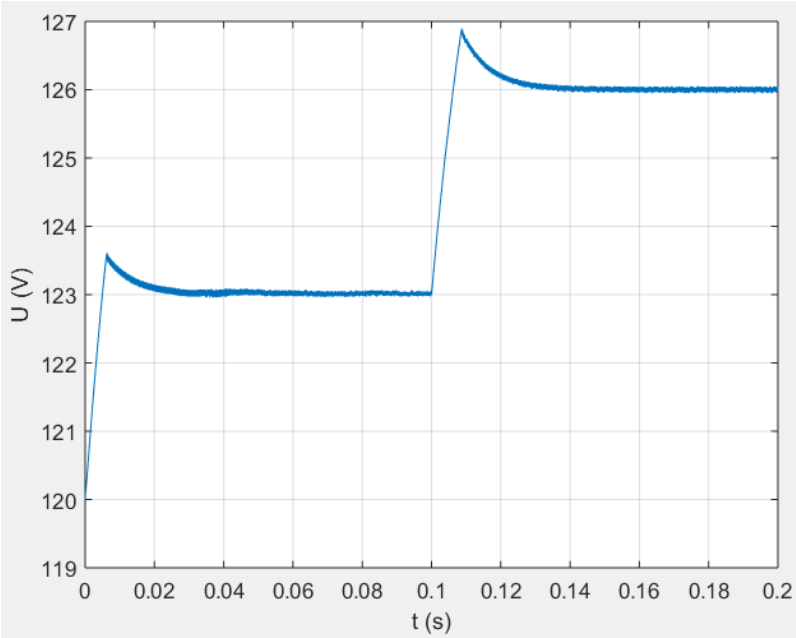

Figure 31. Battery voltage during step response.

The peak-to-peak ripple is 4 A in Figure 30, and the peak-to-peak voltage ripple is *10 mV* in Figure 31. The settling time is *30 ms* which is quite fast, and it indicates that the crossover frequency of the loop gain is sufficient. The crossover frequency is proportional to the settling time. Furthermore, the overshoot is *30 %* of the step change in current which is acceptable. As a conclusion, the total inductor value would increase if two or more converters were to be connected in parallel, but this would provide better tran-

sient behavior, i.e. faster settling times and not as much overshoot. On the other hand, one large converter provides better power quality in terms of ripples excluding transients.

5.3 Cascade control

Current is controlled in the inner loop and voltage in the outer loop in this cascade control. The inner loop is tuned to be a decade faster, for the inner loop must be faster than the outer loop for accurate control. Both the loop gains were solved in 3.1.2, but are repeated here for convenience in Eq. 5.35 and in Eq. 5.36.

$$L_c = G_{cc} R_s {G_{co}}^I \tag{5.35}$$

$$L_v = G_{cv} \frac{G_{cc}}{1+G_{cc}R_s{G_{co}}^I} {G_{co}}^V H_d \tag{5.36}$$

Where G_{cc} is the current controller transfer function, R_s and H_d are the sensing resistors, ${G_{co}}^x$ (x=i,v) is the control-to-output transfer function, G_{cv} is the voltage controller transfer function. ^{I} denotes to a current transfer function and ^{V} to a voltage transfer function. The related control-to-output transfer function ${G_{co}}^x$ are the same as in the separate control case, but the loop gains differ. First, the current loop gain is shown in Fig. 32 and then the voltage loop gain in Fig. 33.

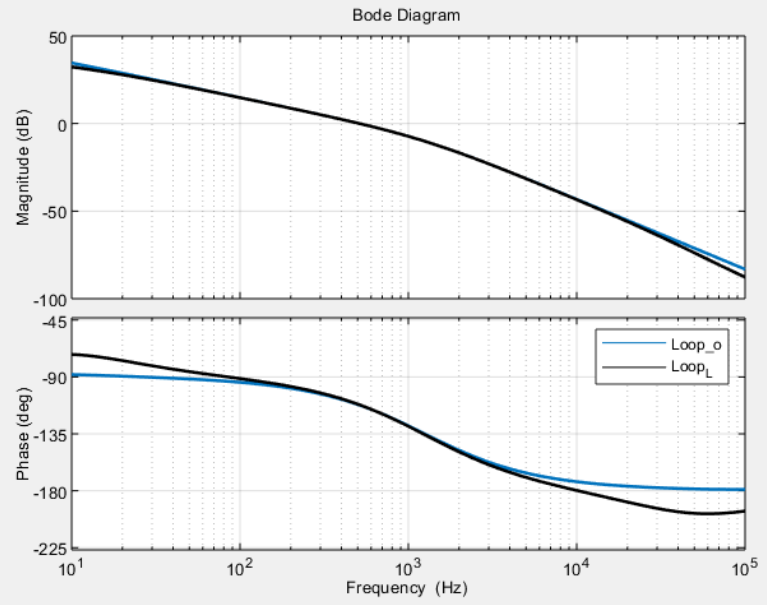

Figure 32. Current loop gains with and without load effect.

There is not much difference in magnitude and gain for the current loop gains as the total loop is considered, therefore only the load affected voltage loop gain is shown in Fig. 33. The inner loop must be faster, and it is tuned to the crossover frequency of *512 Hz*

with phase margin of *68°* and gain margin of *43.7 dB*. The outer loop must have around *50 Hz* crossover frequency for guaranteed operating.

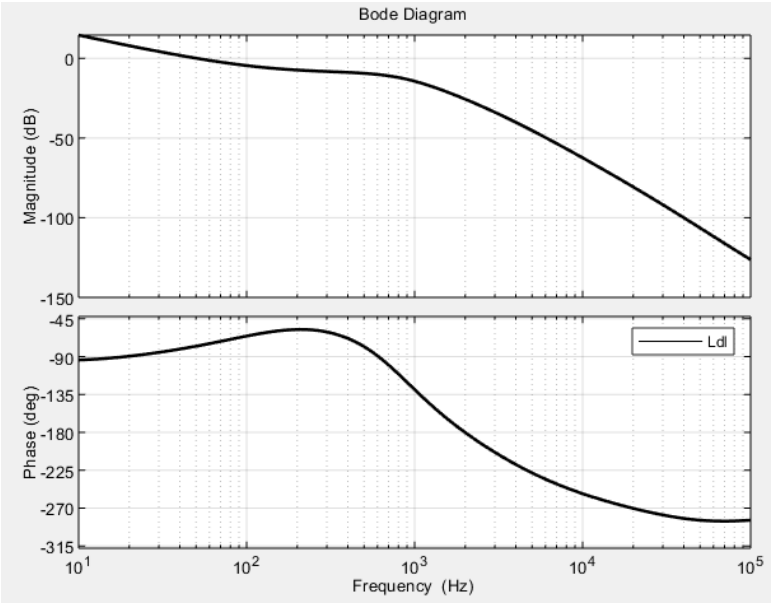

Figure 33. Voltage loop gain with load effect.

The voltage loop gain in Fig. 33 has a crossover frequency of *50.7 Hz* with *108°* PM and *25.6 dB* GM. These values are desirable.

Evaluation of the behavior of the control system is one of the main tasks when designing a converter. Below is a demonstration of the controller's response to a step change from *150 A* to *300 A,* and the battery current and voltage waveforms are in Fig. 34 and in Fig. 35. As in the previous case, the battery model is very simplistic; battery voltage cannot change so rapidly. A more accurate model could be deployed, but the focus is on the control performance, rather than on *100 %* accuracy of the model.

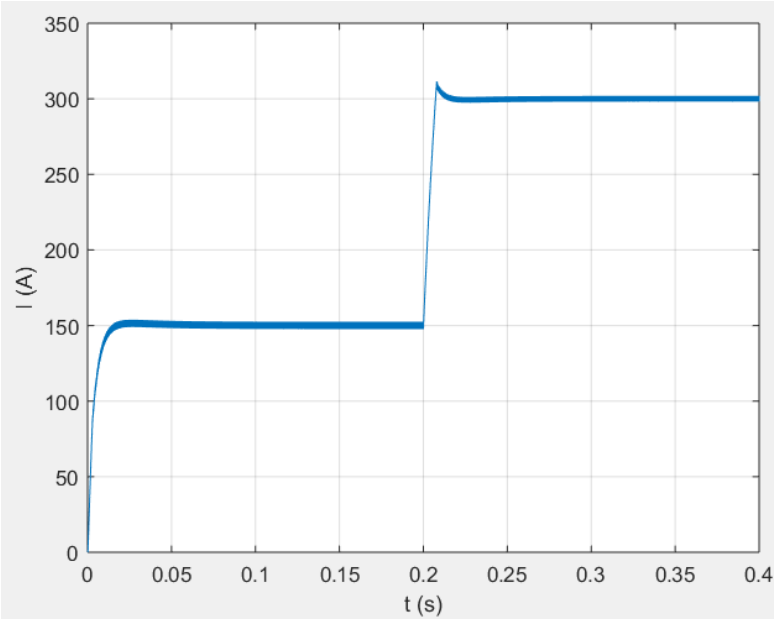

Figure 34. Battery current during a step response.

The current does not have much of overshoot, which is the crossing of the reference value. Furthermore, the settling time is around *20 ms* which is *33 %* faster than the one big buck converter using separate controllers. The current behaves as it should, considering the reference values which are *150 A* and *300 A*.

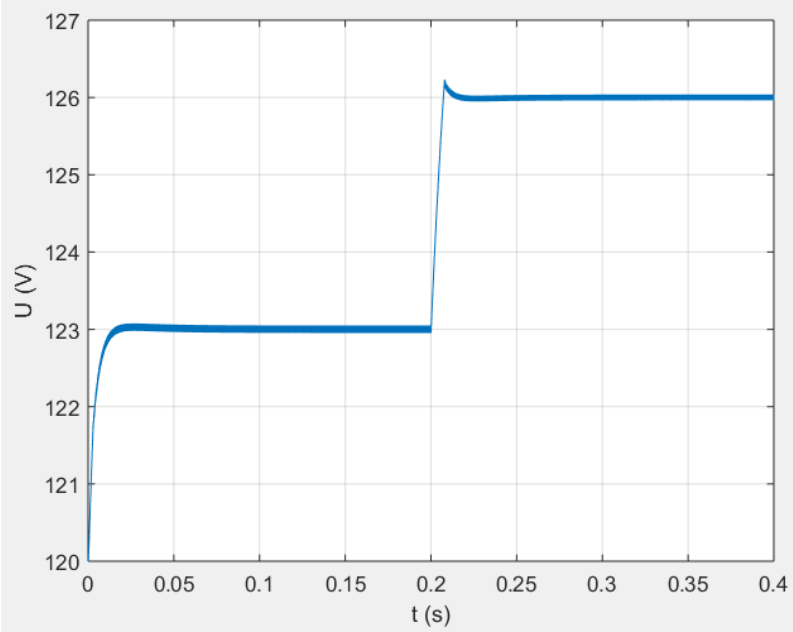

Figure 35. Battery voltage.

The overshoot of the output voltage causes the current to overshoot. The output current is adjusted by changing the output reference voltage which, in turn, adjusts the duty ratio. The peak-to-peak current ripple is *3 A* and for the voltage *8 mV*. This cascade con-

trol controls both variables at the same even if the output current is indirectly controlled. It has better transient behavior than the separate control and almost nonexistent ripples.

Three simulations were presented of which the cascade control is the most accurate because it is based on simultaneous control of the output variables. The inductor for the two-converter topology was not dimensioned for this purpose which is visible on the results. However, if the inductor value is *75 %* of the original value *1.2 mH* for both converters, the peak-to-peak current ripple is only *12 A*. All simulated ripples are shown in Table 2.

Table 2. Peak-to-peak ripples for different controls and topologies.

Variables	Two-converters	One converter (separate)	One converter (cascade)
L-size (mH)	0,95	1,2	1,2
Ip-p,ripple (A)	12	4	3
Up-p,ripple (mV)	300	10	8

The cascade controller was simulated to demonstrate how fast and accurate it could be, but this kind of controller should use the reference current value for the outer loop. Instead of this, the output voltage is controlled in the outer loop, for otherwise the control would be slow and inaccurate for the output current. The separate control is more realistic option in practice and as demonstrated, the topology can be implemented with one large buck converter or with more than one buck converter in parallel. Buck converters in parallel would reduce the stress on the components, improve transient behavior, reduce EMI-problems, but the synchronization should be implemented with practically no delay between converters.

6. PRACTICAL DESIGN OF BATTERY MODULE TESTER

Due to lack of time the building part is postponed to the summer of 2018. This chapter was to describe the process outlines initially, but now it is to detail some of the important design criteria. PI-controller parameter choosing, how to connect an optocoupler to the gate drive of an IGBT and how the PLC is controlled are discussed in this chapter.

6.1 Programmable logic control

The real implementation regarding the controller is done with the PLC which is part of CJ2M-series by Omron. The processor is capable of execution time as low as *40 ns* which really enhances the performance [32]. The idea in the controller implementation is that by using actuators to measure the output voltage and the output current the duty ratio can be controlled using either PI- or PID-controller.

The actual tuning can be done either manually or automatically. PID command includes 3 operands: S (measurement value PV), C (first parameter word) and D (controller output). User needs to define control interval τ, K_p-, I- and D-parameters. The controller adjusts the output according to these values. The derivative control can have a positive impact during transients, but only PI-controller is analyzed in this chapter. The controller transfer function which was used in simulation is shown in Eq. 6.1.

$$G_c = K \cdot \frac{\left(1+\frac{s}{\omega_z}\right)}{s\left(1+\frac{s}{\omega_p}\right)} \tag{6.1}$$

Where K is the DC-gain, ω_p is the crossover frequency of the pole and ω_z is the crossover frequency of the zero. This function has a PI-control transfer function which is the numerator in Eq. 6.1 and a low-pass filter transfer function which is the denominator in Eq. 6.1. It can be modified as below.

$$G_c = G_{PI}G_{LP} = \frac{K\left(1+\frac{s}{\omega_z}\right)}{s} \cdot \frac{1}{\left(1+\frac{s}{\omega_p}\right)}$$

Where G_{PI} is the PI-controller transfer function and G_{LP} is the low-pass filter transfer function. The gains K_p and K_i can be solved by Eq. 6.1 for the voltage controller K is

equal to *316.2*, ω_z is equal to 40π and ω_p is 2778π. First, the PI-controller parameters are solved.

$$G_{PI} = \frac{K\left(1 + \frac{s}{\omega_z}\right)}{s} = \frac{K}{s} + \frac{K}{\omega_z} = \frac{K_i}{s} + K_p$$

$$G_{PI} = \frac{316.2}{s} + \frac{316.2}{40\pi}$$

The integral gain K_i is equal to 316.2 and the proportional gain K_p is equal to 2.52. Since the crossover frequency is equal to 2778π, this filter should attenuate the signals which have a higher frequency.

The current controller has a similar transfer function, expect for the parameters have different values. K is set to *87.1*, the crossover frequency of the zero is equal to 50π and ω_p is 2500π. The gains can be solved similarly as above which results in the integral gain of 87.1 and in the proportional gain of 0.5545. The gain parameters are summed up in Table 3.

Table 3. PI-controller parameters.

Controller	***Voltage controller***	***Current controller***
Proportional gain	2,52	0,5545
Integral gain	316,2	87,1

The PWM is done using a sinking-type I/O module CJ2M-MD211 and its layout, pin numbers and signal types are shown in Figure 36. In practice, this module is connected by an optocoupler to the IGBT gates.

Pin layout	Terminal symbol	Input signal type	Pin	*	Terminal symbol	Input signal type	Pin	*
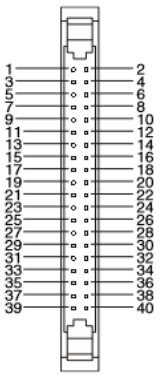	IN00/IN10	24 VDC	1	A1	IN01/IN11	24 VDC	2	B1
		LD+	3	A2		LD+	4	B2
		0 V/LD–	5	A3		0 V/LD–	6	B3
	IN02/IN12	24 VDC	7	A4	IN03/IN13	24 VDC	8	B4
		LD+	9	A5		LD+	10	B5
		0 V/LD–	11	A6		0 V/LD–	12	B6
	IN04/IN14	24 VDC	13	A7	IN05/IN15	24 VDC	14	B7
		LD+	15	A8		LD+	16	B8
		0 V/LD–	17	A9		0 V/LD–	18	B9
	IN06/IN16	24 VDC	19	A10	IN07/IN17	24 VDC	20	B10
		LD+	21	A11		LD+	22	B11
		0 V/LD–	23	A12		0 V/LD–	24	B12
	IN08/IN18	24 VDC	25	A13	IN09/IN19	24 VDC	26	B13
		LD+	27	A14		LD+	28	B14
		0 V/LD–	29	A15		0 V/LD–	30	B15
	OUT00/OUT10	---	31	A16	OUT01/OUT11	---	32	B16
	OUT02/OUT12	---	33	A17	OUT03/OUT13	---	34	B17
	OUT04/OUT14	---	35	A18	OUT05/OUT15	---	36	B18
	Power supply input +V for outputs	---	37	A19	Power supply input +V for outputs	---	38	B19
	COM	---	39	A20	COM	---	40	B20

Figure 36. CJ2M-MD211 connector pin allocations [32].

The power supply of the I/O-module and the optocoupler circuit are connected to the same power supply. The power supply can be within *5-24 V*, but practically it is easier to use *24 V* input voltage for there is a power supply unit available for this voltage level. The PWM outputs [32] are OUT4/OUT14 and OUT5/OUT15 and the maximum frequency is up to *32.8 kHz*.

6.2 Optocouplers

Optocouplers are used in applications such as gate driving, current sensing, voltage sensing and digital communication, for example, isolated CAN bus digital communication. Their main feature is galvanic isolation which improves safety of the system. One desired feature is their high efficiency. [33]

Optocouplers are used in a way the same as transformers, the main idea is to isolate the primary "windings" from the secondary "windings". In practice, the control circuit is located on one side of the optocoupler and the load circuit on the other side. The primary side includes usually a light-emitting diode (LED), while the secondary side is equipped with a photo-transistor. The actual power transfer happens optically, in contrast to transformers. [34]

The PLC is the PWM source in this configuration and this PWM signal is transmitted via an optocoupler PCB to the IGBT driver circuit which is already built by the manufacturer. The pins for the used optocoupler are shown in Fig. 37.

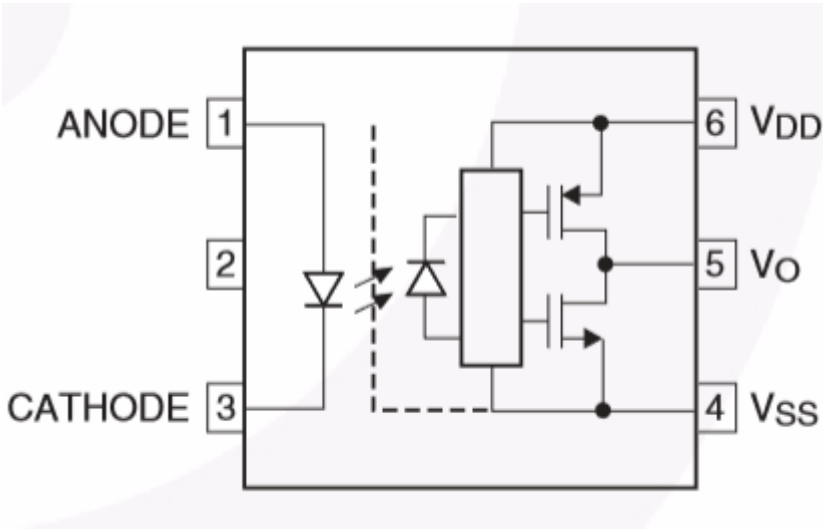

Figure 37. Optocoupler pins [35].

The primary side includes only a LED while the secondary side has the supply voltage pins, V_{DD} and V_{SS}, and the actual output V_O. The PCB design is straight forward since only a few surface mounted devices are required.

A front-end resistor can be determined by Eq. 6.2. If the voltage over the LED V_F is 1.1 *V* and the power supply is *5 V*, the input current can be limited using a resistor. The minimum value for the input current to turn on the LED is *10 mA*. The resistor value can be calculated as in Eq. 6.2. [35]

$$R_{max} = \frac{V_{supply} - V_{F,min}}{I_{in,min}} \tag{6.2}$$

$$R_{max} = \frac{5\ V - 1.1\ V}{10\ mA} = 390\ \Omega$$

This is the maximum value for if the resistor value is greater, then the minimum input turn-on current cannot be achieved. If the power supply is *24 V*, then the maximum resistor value would be *2.3 k*Ω, *1.8 k*Ω standard value is available. Furthermore, a ferrite bead [36] could be placed in series with the input resistor to reduce high frequency noise/spikes in the spectrum. According to the datasheet [36], if the rated DC current is equal to *15 mA*, the correct value for the inductance would be *12 μH*. The threshold voltage to the IGBT is *6 V* while the supply voltage is *24 V* which is also the output voltage of the optocoupler, so a resistor divider must be used. The first output resistor R_1 is *100* Ω which allows the latter to be dimensioned Eq 6.3.

$$I = \frac{U}{R_1 + R_2} = \frac{U_1}{R_1} = \frac{U_2}{R_2}$$

$$U_2 = \frac{R_2 U}{R_1 + R_2}$$

$$U_2(R_1 + R_2) = R_2 U$$

$$R_2 = \frac{R_1 U_2}{U - U_2} \tag{6.3}$$

$$R_2 = \frac{100\ \Omega \cdot 6\ V}{24\ V - 6\ V}$$

$$R_2 = 33.3\ \Omega$$

33 Ω is a standard resistor value which is chosen. The resulting schematics is presented in Fig. 38.

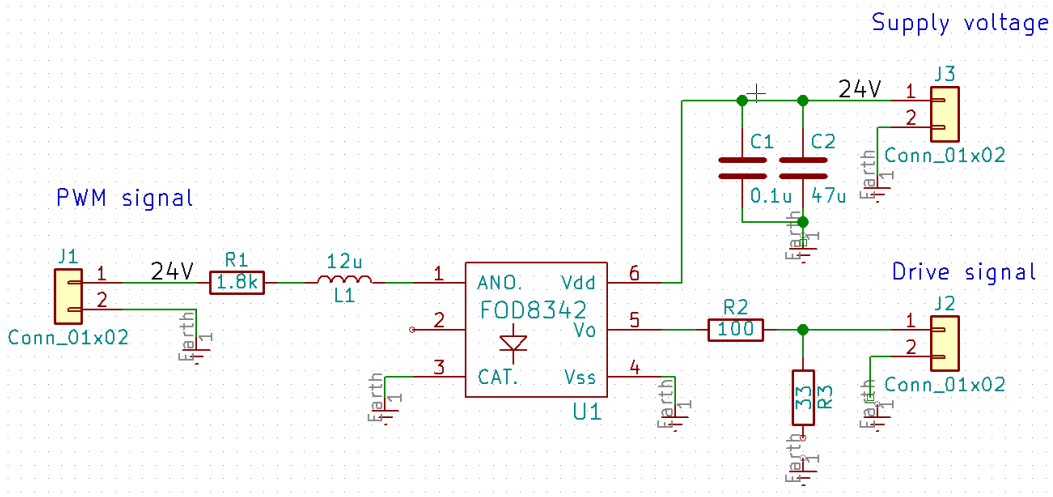

Figure 38. Optocoupler coupling schematics.

In EMC-perspective, it is important to separate analog/digital and power grounds. A stiff voltage source is preferable to have as well as the input filtering. This is done with the combination of a resistor and a ferrite bead. The resistor is used for current limiting and the ferrite bead for filtering the high frequency signals.

The actual footprint layout is shown in Figure 39. The main design issues are to minimize current loops and use copper only as much as needed. *J1*, *J2* and *J3* are connector terminals, and all the other components are surface mount devices excluding *U1* which is the optocoupler.

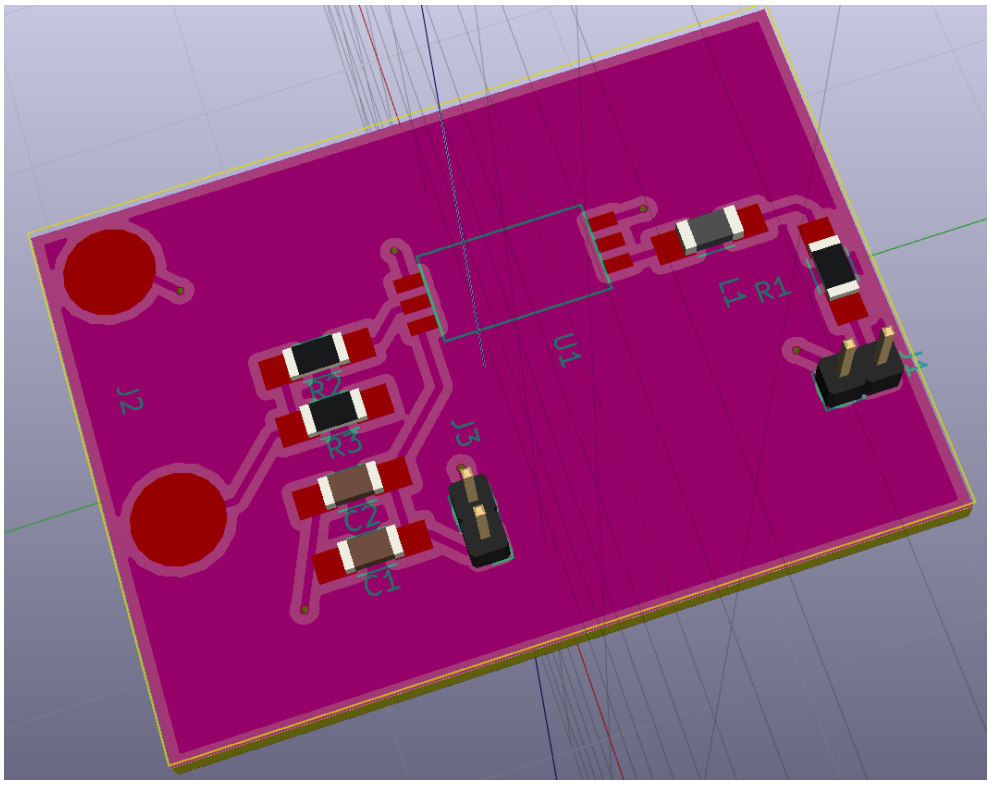

Figure 39. PCB front layout.

On the front side of the board there is only copper tracks that connect the components which could be made a bit wider for to minimize the resistance and inductance. The back side is filled with copper, but there are also some areas that are not filled, because the output pins are drilled and mounted straight to the IGBT drive circuit. The ground connections are connected through vias to the bottom layer.

The principle of optocoupler use in IGBT drive is shown in Fig. 40. However, the IGBT drives are finished products. Only the gate signal transfer through an optocoupler is designed.

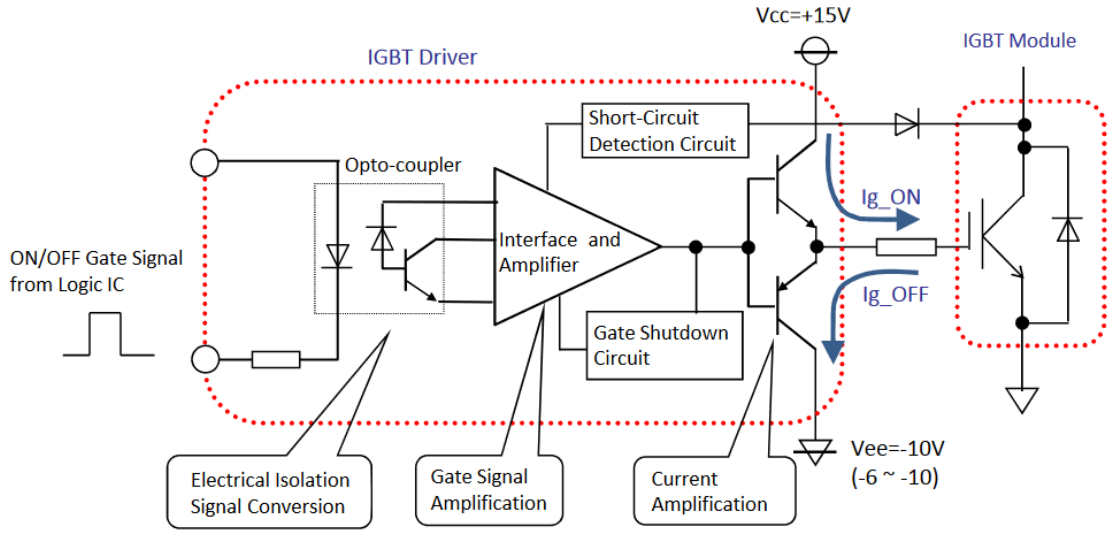

Figure 40. IGBT drive circuit [37].

The optocoupler are used to provide galvanic isolation between the PLC and the IGBT drives and to provide reliable transmission path without delay. Optocouplers could also be used for measuring feedback signals, but in this application the optocouplers are used for gate driving.

7. CONCLUSIONS

The battery modules which are tested are *24 V* Li-ion batteries, and these modules are used as an optional or main power supply. These modules must be tested to make sure the products which use these modules can be sold and for the customers to be safe. This was the motive for the whole study to introduce different options for the battery module tester to be able to fulfill requirements for current and voltage levels. Batteries and their modeling, converter components, buck converter control and alternatives for the battery module tester were reviewed in this thesis.

Batteries are generally complicated to present as mathematical functions since the voltage dependency is usually not linear. To model a battery, some capacitance and internal resistance can be included in the model. Very simple models, such as the linear model, include only internal resistance of the battery. This simplifies the analysis greatly and all the required data is available for commercial batteries. The linear model was used in the simulations for, in the end, the reference of the controller is responsible for adjusting the output variable.

There are many ways how to build a device for battery testing even if only three were listed in this thesis. This kind of power source could be implemented with a different topology: isolated or non-isolated, and structure. However, the isolated converters were neglected for it was decided to use a transformer in the AC-side. The basic idea is to decrease the voltage to a level which is controllable in the range of *20 – 125 V*. The alternatives in this thesis were buck converter, active rectifier and commercial battery chargers. The benefits of using the active rectifier are lower current stress per phase and bi-directional power flow. However, for a practical implementation a buck converter would still be required after the active rectifier for the voltage range is too wide. The commercial battery chargers are an interesting choice, but the lack of knowledge of control and price in this application excluded this option. The buck converter was selected for this purpose, since only the passive components, i.e. capacitor and inductor, are needed and control is simple.

Current or voltage or both at the same time can be controlled in the buck converter topology. The easiest way is to control voltage, since current measuring is not that simple. Current can be measured using a current transformer or a current measuring resistor. To enhance the performance of the control, cascade control would be the best choice, but the inner loop should be much faster than the outer loop and the current reference should be the outer loop, for this value is the primary controlled variable in this applica-

tion, i.e. the reference value. This leads to a conflict, and it disqualifies the cascade control. Separate control of the output voltage and current would be an adequate choice.

The current control is the most critical issue in this application, which means that if the current is controlled only by a voltage reference there is no measured knowledge what is the actual current. For this reason, both, voltage and current must be controlled. The separate control provides knowledge of both output variables which can be used as a feedback to control the current to the level which is required by the program. Otherwise, the battery model should be very accurate and still it would be unsure to control the output current with only a voltage reference.

The BMSs of the battery modules are connected to the PLC via CAN-bus. In this application the function of the BMSs is simply monitor the battery modules while the PLC controls the battery modules and limits the supply to the battery modules in hazardous situations. The control must be implemented in a way that the current, temperature and voltage limits, which are defined by the manufacturer, cannot be exceeded either limiting or shutting down the supply. The next step for this process is to build the battery module tester.

8. REFERENCES

[1] D. Linden, T.B. Reddy, *Linden's Handbook of batteries*, 4th ed. McGraw-Hill, New York, 2010.

[2] “Toyota Develops World's First Behavior Observation Method,” [cited 6/2/2018]. [Online]. Available at: https://newsroom.toyota.co.jp/en/detail/14326042

[3] J.T. Warner, *The Handbook of Lithium-Ion Battery Pack Design: Chemistry, Components, Types and Terminology*, Elsevier Science, US, 2015.

[4] A.R. Sparacino, G.F. Reed, R.J. Kerestes, B.M. Grainger, Z.T. Smith, Survey of battery energy storage systems and modeling techniques, 2012 IEEE Power and Energy Society General Meeting, IEEE, pp. 1-8.

[5] M.T. Lawder, B. Suthar, P.W.C. Northrop, S. De, C.M. Hoff, O. Leitermann, M.L. Crow, S. Santhanagopalan, V.R. Subramanian, Battery Energy Storage System (BESS) and Battery Management System (BMS) for Grid-Scale Applications, Proceedings of the IEEE, Vol. 102, Iss. 6, 2014, pp. 1014-1030.

[6] W. Waag, S. Käbitz, D.U. Sauer, Experimental investigation of the lithium-ion battery impedance characteristic at various conditions and aging states and its influence on the application, Applied Energy, Vol. 102, 2013, pp. 885-897.

[7] T. Suntio, *Dynamic profile of switched-mode converter: modeling, analysis and control*, Wiley-VCH, 2009.

[8] X.H. Zhang, The Research of "Constant Current First, Constant Voltage After" Close-Loop Control Charging Tactics of High Frequency Charger, Applied Mechanics and Materials, Vol. 494-495, Iss. Current Development of Mechanical Engineering and Energy, 2014, pp. 1556-1560.

[9] M. Chen, G.A. Rincon-Mora, Accurate, Compact, and Power-Efficient Li-Ion Battery Charger Circuit, IEEE Transactions on Circuits and Systems II: Express Briefs, Vol. 53, Iss. 11, 2006, pp. 1180-1184.

[10] S. Bacha, I. Munteanu, A.I. Bratcu, *Power Electronic Converters Modeling and Control: with Case Studies*, 2014th ed. Springer, London, 2014, 458 p.

[11] R.W. Erickson, D. Maksimovi , *Fundamentals of power electronics*, 2nd ed. Kluwer Academic, Norwell (MA), 2007.

[12] M. Liserre, F. Blaabjerg, S. Hansen, Design and control of an LCL-filter-based three-phase active rectifier, IEEE Transactions on Industry Applications, Vol. 41, Iss. 5, 2005, pp. 1281-1291.

[13] M.H. Antchev, *Technologies for Electrical Power Conversion, Efficiency, and Distribution : Methods and Processes*, IGI Global, Hershey, 2009.

[14] M. Rashid, *Power Electronics Handbook (4)*, Elsevier Science, Saint Louis, 2017.

[15] S.M. Sharkh, M.A. Abu-Sara, G.I. Orfanoudakis, B. Hussain, *Power Electronic Converters for Microgrids*, 1st ed. IEEE Press, Singapore, 2014.

[16] N. Mohan, W.P. Robbins, T.M. Undeland, *Power electronics: converters, applications and design*, 3rd ed. Wiley, Hoboken (NJ), 2003.

[17] "Tesla A Bit About Batteries," [cited 16/5/2018]. [Online]. Available at: https://www.tesla.com/fi_FI/blog/bit-about-batteries

[18] "Powerfinn 3200 W battery charger datasheet," [cited 15/10/2017]. [Online]. Available at: http://www.powerfinn.fi/3200W

[19] "Infineon FS300R12KE3 IGBT module datasheet," [cited 2/4/2018]. [Online]. Available at: https://www.infineon.com/dgdl/Infineon-FS300R12KE3-DS-v03_01-en_de.pdf?fileId=db3a304412b407950112b4311ff85394

[20] "Fairchild Electromagnetic Interference (EMI) in Power Supplies," [cited 4/4/2018]. [Online]. Available at: https://www.fairchildsemi.com/technical-articles/Electromagnetic-Interference-EMI-in-Power-Supplies.pdf

[21] Y. Bavafa-Toosi, *Introduction to Linear Control Systems*, Academic Press, San Diego, 2017.

[22] R.C. Dorf, R.H. Bishop, *Modern control systems*, 11th ed. Pearson/Prentice Hall, Upper Saddle River (NJ), 2008.

[23] T. Messo. *Factors Affecting Stable Operation of Grid-Connected Three-Phase Photovoltaic Inverters*. PhD thesis, Tampere University of Technology, 2014.

[24] K.J. Åström, R.M. Murrey, *Feedback systems: an introduction for scientists and engineers*, illustrat ed. Princeton University Press, Princeton, NJ, 2010.

[25] “Fujitsu Fast Pulse Width Modulation (FPWM) Technology for DC-DC Converter, Featuring High-speed Response with a Clock-Synchronized Comparator Control method,” [cited 10/2/2018]. [Online]. Available at: http://www.fujitsu.com/downloads/EDG/binary/pdf/find/30-3e/4.pdf

[26] W. Kester, W. Jung, J. Bryant, B. Chestnut, “Hardware Design Techniques,” [cited 27/2/2018]. [Online]. Available at: http://www.analog.com/media/en/training-seminars/design-handbooks/Practical-Design-Techniques-Power-Thermal/Section8.pdf

[27] K. Armstrong, “Design Techniques for EMC Part 3 – Filtering and Suppressing Transients,” [cited 27/2/2018]. [Online]. Available at: http://www.cherryclough.com/media/file/Design%20techniques/Part%203%20text%20and%20graphics,%2021%20May%2009.pdf

[28] “Kemet EMI Cores,” [cited 16/5/2018]. [Online]. Available at: http://www.kemet.com/EMI%20Cores?value=EMI%20Cores

[29] W. Kester, J. Bryant, “Grounding in high speed systems,” [cited 3/3/2018]. [Online]. Available: http://www.analog.com/media/en/training-seminars/design-handbooks/high-speed-design-tech-sect7b.pdf

[30] “Vishay Aluminum Capacitors datasheet,” [cited 31/1/2018]. [Online]. Available at: https://www.mouser.com/ds/2/427/80d-102349.pdf

[31] G. Garcera, E. Figueres, M. Pascual, J.M. Benavent, Robust model following control of parallel buck converters, IEEE Transactions on Aerospace and Electronic Systems, Vol. 40, Iss. 3, 2004, pp. 983-997.

[32] CJ-series CJ2M CPU Units, Pulse I/O Modules: CJ2M-CPU3 /-CPU1 / -MD21 , Omron, available at: http://www.ia.omron.com/data_pdf/cat/cj2m-cpu3__-cpu1_-md21__ds_e_11_3_csm2201.pdf?id=2712

[33] H. L. Chen, “Optocouplers Help Promote Safe, Efficient EV Charging Stations,” [cited 7/2/2018]. [Online]. Available at: http://www.electronicdesign.com/power/optocouplers-help-promote-safe-efficient-ev-charging-stations

[34] “Vishay Optocoupler Product Portfolio,” [cited 7/2/2018]. [Online]. Available at: http://www.vishay.com/docs/49624/_pl0475.pdf

[35] “Onsemi FOD8342, FOD8342T optocoupler datasheet,” [cited 4/2/2018]. [Online]. Available at: http://www.onsemi.com/pub/Collateral/FOD8342-D.pdf

[36] “Vishay ILBB-0603 Ferrite Bead Datasheet,” [cited 4/2/2018]. [Online]. Available at: https://www.vishay.com/docs/34024/ilbb0603.pdf

[37] “ISAHAYA ELECTRONICS IGBT Drivers,” [cited 17/5/2018]. [Online]. Available at: http://www.idc-com.cn/html_en/product/pdf/IGBT_ApplicationManual_E.pdf

APPENDIX A: BUCK CALCULATIONS (VFVO)

On-equations:

$$v_{in} - i_{c_{in}} r_{c_{in}} - v_{C_{in}} = 0$$

$$i_{c_{in}} = \frac{v_{in} - v_{C_{in}}}{r_{c_{in}}}$$

$$\frac{dv_{c_{in}}}{dt} = \frac{1}{r_{c_{in}} C}\left(v_{in} - v_{C_{in}}\right)$$

$$i_L - i_{C_{out}} - i_o = 0$$

$$i_{C_{out}} = i_L - i_o$$

$$\frac{dv_{c_{out}}}{dt} = \frac{1}{C}(i_L - i_o)$$

$$v_o = v_{C_{out}} + r_{C_{out}} \cdot (i_L - i_o)$$

$$v_{in} - i_L \cdot (r_{sw} + r_L) - v_{L-on} - v_o = 0$$

$$v_{in} - i_L \cdot (r_{sw} + r_L) - v_{L-on} - v_{C_{out}} - r_{C_{out}} \cdot (i_L - i_o) = 0$$

$$v_{L-on} = v_{in} - i_L \cdot (r_{sw} + r_L) - v_{C_{out}} - r_{C_{out}} \cdot (i_L - i_o)$$

$$\frac{di_{L-on}}{dt} = \frac{1}{L}\left(v_{in} - \left(r_{sw} + r_L + r_{C_{out}}\right)i_L - v_{C_{out}} + r_{C_{out}} i_o\right)$$

$$i_{in} = i_L + i_{c_{in}}$$

$$i_{in} = i_L + \frac{1}{r_{c_{in}}} v_{in} - \frac{1}{r_{c_{in}}} v_{C_{in}}$$

Off-equations:

$$v_{in} - i_{c_{in}} r_{c_{in}} - v_{C_{in}} = 0$$

$$i_{c_{in}} = \frac{v_{in} - v_{C_{in}}}{r_{c_{in}}}$$

$$\frac{dv_{c_{in}}}{dt} = \frac{1}{r_{c_{in}} C}\left(v_{in} - v_{C_{in}}\right)$$

$$i_L - i_{C_{out}} - i_o = 0$$

$$i_{C_{out}} = i_L - i_o$$

$$\frac{dv_{c_{out}}}{dt} = \frac{1}{C}(i_L - i_o)$$

$$v_o = v_C + r_C \cdot (i_L - i_o)$$

$$v_d + i_L \cdot (r_d + r_L) + v_L + v_o = 0$$

$$v_L = -v_d - (r_d + r_L)i_L - v_{C_{out}} - r_{C_{out}}(i_L - i_o)$$

$$\frac{di_L}{dt} = \frac{1}{L}\left(-v_d - \left(r_d + r_L + r_{C_{out}}\right)i_L - v_{c_{out}} + r_{C_{out}}i_o\right)$$

$$i_{in} = i_{c_{in}}$$

$$i_{in} = \frac{1}{r_{c_{in}}}v_{in} - \frac{1}{r_{c_{in}}}v_{C_{in}}$$

Average state space:

$$\frac{di_L}{dt} = d \cdot \frac{di_{L-on}}{dt} + d' \cdot \frac{di_{L-off}}{dt}$$

$$\frac{di_L}{dt} = d \cdot \frac{1}{L}\left(v_{in} - \left(r_{sw} + r_L + r_{C_{out}}\right)i_L - v_{C_{out}} + r_{C_{out}}i_o\right) + d' \cdot \frac{1}{L}\left(-v_d - \left(r_d + r_L + r_{C_{out}}\right)i_L - v_{c_{out}} + r_{C_{out}}i_o\right)$$

$$\frac{di_L}{dt} = \frac{1}{L}\left(dv_{in} - d\left(r_{sw} + r_L + r_{C_{out}}\right)i_L - dv_{C_{out}} + dr_{C_{out}}i_o - d'v_d - d'\left(r_d + r_L + r_{C_{out}}\right) \cdot i_L - d'v_{c_{out}} + d'r_{C_{out}}i_o\right)$$

$$\frac{d\langle i_L\rangle}{dt} = \frac{1}{L}\left(d\langle v_{in}\rangle - \left(dr_{sw} + r_L + r_{C_{out}} + d'r_d\right)\langle i_L\rangle - \langle v_{c_{out}}\rangle + r_{C_{out}}\langle i_o\rangle - d'v_d\right)$$

$$\frac{dv_c}{dt} = d \cdot \frac{dv_{c-on}}{dt} + d' \cdot \frac{dv_{c-off}}{dt}$$

$$\frac{dv_{c_{out}}}{dt} = d\frac{1}{C_{out}}(i_L - i_o) + d'\frac{1}{C_{out}}(i_L - i_o)$$

$$\frac{d\langle v_{c_{out}}\rangle}{dt} = \frac{1}{C_{out}}\langle i_L\rangle - \frac{1}{C_{out}}\langle i_o\rangle$$

$$\frac{dv_{c_{in}}}{dt} = d\left(\frac{1}{r_{c_{in}}C}\left(v_{in} - v_{C_{in}}\right)\right) + d'\left(\frac{1}{r_{c_{in}}C}\left(v_{in} - v_{C_{in}}\right)\right)$$

$$\frac{d\langle v_{c_{in}}\rangle}{dt} = \frac{1}{r_{c_{in}}C_{in}}\left(\langle v_{in}\rangle - \langle v_{C_{in}}\rangle\right)$$

$$i_{in} = d \cdot i_{in-on} + d' \cdot i_{in-off}$$

$$i_{in} = \mathrm{d}\left(i_L + \frac{1}{r_{c_{in}}}v_{in} - \frac{1}{r_{c_{in}}}v_{C_{in}}\right) + d'\left(\frac{1}{r_{c_{in}}}v_{in} - \frac{1}{r_{c_{in}}}v_{C_{in}}\right)$$

$$\langle i_{in}\rangle = d\langle i_L\rangle + \frac{1}{r_{c_{in}}}\langle v_{in}\rangle - \frac{1}{r_{c_{in}}}\langle v_{C_{in}}\rangle$$

$$v_o = d \cdot i_{o-on} + d' \cdot i_{o-off}$$

$$v_o = d \cdot \left(v_{C_{out}} + r_{C_{out}} \cdot (i_L - i_o)\right) + d' \cdot \left(v_{C_{out}} + r_{C_{out}} \cdot (i_L - i_o)\right)$$

$$\langle v_o\rangle = \langle v_{C_{out}}\rangle + r_{C_{out}}\langle i_L\rangle - r_{C_{out}}\langle i_o\rangle$$

Steady-state operation point:

$$\frac{dv_{c_{in}}}{dt} = \frac{1}{r_{c_{in}}C_{in}}\left(v_{in} - v_{C_{in}}\right)$$

$$0 = \left(V_{in} - V_{C_{in}}\right)$$

$$V_{in} = V_{C_{in}}$$

$$\frac{dv_{c_o}}{dt} = \frac{1}{C}(i_L - i_o)$$

$$I_L = I_o$$

$$I_{in} = DI_L + \frac{1}{r_{c_{in}}}\mathrm{V}_{in} - \frac{1}{r_{c_{in}}}\mathrm{V}_{c_{in}}$$

Since V_{in} is equal to V_{cin}

$$I_{in} = DI_L$$

$$V_o = V_C + r_C \cdot (I_L - I_o)$$

And I_L equals to I_o, so:

$$V_o = V_C$$

$$\frac{di_L}{dt} = \frac{1}{L}\left(d\langle v_{in}\rangle - (dr_{sw} + r_L + r_C + d'r_d)\langle i_L\rangle - \langle v_{c_{out}}\rangle + r_{C_{out}}\langle i_o\rangle - d'v_d\right)$$

$$0 = \frac{1}{L}\left(DV_{in} - DI_L \cdot r_{sw} - I_L \cdot \left(r_L + \cancel{r_{C_{out}}}\right) - D'I_L \cdot r_d - V_{c_{out}} + \cancel{r_{C_{out}}} I_o - D'v_d\right)$$

$$0 = DV_{in} - DI_L r_{sw} - I_L r_L - (1-D)I_L r_d - V_{c_{out}} - (1-D)v_d$$

$$DV_{in} - DI_L r_{sw} + DI_L r_d + Dv_d = I_L r_L + I_L r_d + V_{c_{out}} + v_d$$

$$D = \frac{(r_L + r_d)I_L + V_{c_{out}} + v_d}{V_{in} - (r_{sw} - r_d)I_L + v_d}$$

Substituting the steady state values D becomes:

$$D = \frac{(r_L + r_d)I_o + V_o + v_d}{V_{in} - (r_{sw} - r_d)I_o + v_d}$$

The state, input and output vectors are:

$$\boldsymbol{x} = [\hat{\imath}_L \quad \hat{v}_{C_{in}} \quad \hat{v}_{C_{out}}]^T$$

$$\boldsymbol{u} = [\hat{v}_{in} \quad \hat{\imath}_o \quad \hat{d}]^T$$

$$\boldsymbol{y} = [\hat{\imath}_{in} \quad \hat{v}_o]^T$$

Linearization:

$$\frac{d\langle v_{c_{in}}\rangle}{dt} = \frac{1}{r_{c_{in}}C_{in}}\langle v_{in}\rangle - \frac{1}{r_{c_{in}}C_{in}}\langle v_{C_{in}}\rangle$$

$$\frac{di_L}{dt} = \frac{1}{L}\left(dv_{in} - dr_{sw}i_L - \left(r_L + r_{C_{out}}\right)i_L - (1-d)r_d i_L - v_{c_{out}} + r_{C_{out}}i_o - (1-d)v_d\right)$$

$$\frac{d\hat{\imath}_L}{dt} = \frac{1}{L}\left(D\hat{v}_{in} - \left(Dr_{sw} + r_L + r_{C_{out}} + D'r_d\right)\hat{\imath}_L - \hat{v}_{c_{out}} + r_{C_{out}}\hat{\imath}_o + (V_{in} - r_{sw}I_o + r_d I_o + v_d)\hat{d}\right)$$

$$\frac{d\hat{\imath}_L}{dt} = \frac{1}{L}\left(D\hat{v}_{in} - R_1\hat{\imath}_L - \hat{v}_{c_{out}} + r_{C_{out}}\hat{\imath}_o + R_2\hat{d}\right)$$

$$\frac{d\hat{v}_{c_{in}}}{dt} = \frac{1}{r_{c_{in}}C_{in}}\hat{v}_{in} - \frac{1}{r_{c_{in}}C_{in}}\hat{v}_{c_{in}}$$

$$\frac{d\hat{v}_{c_{out}}}{dt} = \frac{1}{C_{out}}(\hat{\imath}_L - \hat{\imath}_o)$$

$$\hat{\imath}_{in} = D\hat{\imath}_L + \frac{1}{r_{c_{in}}}\hat{v}_{in} - \frac{1}{r_{c_{in}}}\hat{v}_{C_{in}} + I_L\hat{d}$$

$$\hat{v}_o = \hat{v}_{C_{out}} + r_{C_{out}} \cdot (\hat{\imath}_L - \hat{\imath}_o)$$

In which

$$R_1 = Dr_{sw} + r_L + r_{C_{out}} + D'r_d$$

$$R_2 = V_{in} - r_{sw}I_o + r_dI_o + v_d$$

In matrix format:

$$\frac{d}{dt}\begin{bmatrix}\hat{\imath}_L \\ \hat{v}_{C_{in}} \\ \hat{v}_{C_{out}}\end{bmatrix} = \begin{bmatrix}-\frac{R_1}{L} & 0 & -\frac{1}{L} \\ 0 & -\frac{1}{r_{c_{in}}C_{in}} & 0 \\ \frac{1}{C_{out}} & 0 & 0\end{bmatrix}\begin{bmatrix}\hat{\imath}_L \\ \hat{v}_{C_{in}} \\ \hat{v}_{C_{out}}\end{bmatrix} + \begin{bmatrix}\frac{D}{L} & \frac{r_{c_{out}}}{L} & \frac{R_2}{L} \\ \frac{1}{r_{c_{in}}C_{in}} & 0 & 0 \\ 0 & -\frac{1}{C_{out}} & 0\end{bmatrix}\begin{bmatrix}\hat{v}_{in} \\ \hat{\imath}_o \\ \hat{d}\end{bmatrix}$$

$$\begin{bmatrix}\hat{\imath}_{in} \\ \hat{v}_o\end{bmatrix} = \begin{bmatrix}D & -\frac{1}{r_{c_{in}}} & 0 \\ r_{C_{out}} & 0 & 1\end{bmatrix}\begin{bmatrix}\hat{\imath}_L \\ \hat{v}_{C_{in}} \\ \hat{v}_{C_{out}}\end{bmatrix} + \begin{bmatrix}\frac{1}{r_{c_{in}}} & 0 & I_o \\ 0 & -r_{C_{out}} & 0\end{bmatrix}\begin{bmatrix}\hat{v}_{in} \\ \hat{\imath}_o \\ \hat{d}\end{bmatrix}$$

$$\boldsymbol{A} = \begin{bmatrix}-\frac{R_1}{L} & 0 & -\frac{1}{L} \\ 0 & -\frac{1}{r_{c_{in}}C_{in}} & 0 \\ \frac{1}{C_{out}} & 0 & 0\end{bmatrix}, \boldsymbol{B} = \begin{bmatrix}\frac{D}{L} & \frac{r_{c_{out}}}{L} & \frac{R_2}{L} \\ \frac{1}{r_{c_{in}}C_{in}} & 0 & 0 \\ 0 & -\frac{1}{C_{out}} & 0\end{bmatrix}$$

$$\boldsymbol{C} = \begin{bmatrix}D & -\frac{1}{r_{c_{in}}} & 0 \\ r_{C_{out}} & 0 & 1\end{bmatrix}, \boldsymbol{D} = \begin{bmatrix}\frac{1}{r_{c_{in}}} & 0 & I_o \\ 0 & -r_{C_{out}} & 0\end{bmatrix}$$

APPENDIX B: BUCK CALCULATIONS (VFCO)

On-equations:

$$v_{in} - i_{c_{in}} r_{c_{in}} - v_{C_{in}} = 0$$

$$i_{c_{in}} = \frac{v_{in} - v_{C_{in}}}{r_{c_{in}}}$$

$$\frac{dv_{c_{in}}}{dt} = \frac{1}{r_{c_{in}} C_{in}} \left(v_{in} - v_{C_{in}}\right)$$

$$v_o - v_{C_{out}} - r_{C_{out}} i_{C_{out}} = 0$$

$$i_{C_{out}} = \frac{1}{r_{C_{out}}} v_o - \frac{1}{r_{C_{out}}} v_{C_{out}}$$

$$\frac{dv_{c_{out}}}{dt} = \frac{1}{r_{c_{out}} C_{out}} v_o - \frac{1}{r_{c_{out}} C_{out}} v_{C_{out}}$$

$$i_L - i_{C_{out}} - i_o = 0$$

$$i_o = i_L - i_{C_{out}}$$

$$i_o = i_L - \frac{1}{r_{C_{out}}} v_o + \frac{1}{r_{C_{out}}} v_{C_{out}}$$

$$v_{in} - i_L \cdot (r_{sw} + r_L) - v_L - v_o = 0$$

$$v_L = v_{in} - i_L \cdot (r_{sw} + r_L) - v_o$$

$$\frac{di_{L-on}}{dt} = \frac{1}{L} (v_{in} - i_L \cdot (r_{sw} + r_L) - v_o)$$

$$i_{in} = i_L + i_{c_{in}}$$

$$i_{in} = i_L + \frac{1}{r_{c_{in}}} v_{in} - \frac{1}{r_{c_{in}}} v_{C_{in}}$$

Off-equations:

$$v_{in} - i_{c_{in}} r_{c_{in}} - v_{C_{in}} = 0$$

$$i_{c_{in}} = \frac{v_{in} - v_{C_{in}}}{r_{c_{in}}}$$

$$\frac{dv_{c_{in}}}{dt} = \frac{1}{r_{c_{in}}C}\left(v_{in} - v_{C_{in}}\right)$$

$$v_o - v_{C_{out}} - r_{C_{out}} i_{C_{out}} = 0$$

$$i_{C_{out}} = \frac{1}{r_{C_{out}}} v_o - \frac{1}{r_{C_{out}}} v_{C_{out}}$$

$$\frac{dv_{C_{out}}}{dt} = \frac{1}{r_{c_{out}} C_{out}} v_o - \frac{1}{r_{c_{out}} C_{out}} v_{C_{out}}$$

$$i_L - i_{C_{out}} - i_o = 0$$

$$i_o = i_L - i_{C_{out}}$$

$$i_o = i_L - \frac{1}{r_{C_{out}}} v_o + \frac{1}{r_{C_{out}}} v_{C_{out}}$$

$$v_d + i_L \cdot (r_d + r_L) + v_L + v_o = 0$$

$$v_L = -v_d - (r_d + r_L) i_L - v_o$$

$$\frac{di_L}{dt} = \frac{1}{L}(-v_d - (r_d + r_L) i_L - v_o)$$

$$i_{in} = i_{c_{in}}$$

$$i_{in} = \frac{1}{r_{c_{in}}} v_{in} - \frac{1}{r_{c_{in}}} v_{C_{in}}$$

Average state space:

$$\frac{di_L}{dt} = d \cdot \frac{di_{L-on}}{dt} + d' \cdot \frac{di_{L-off}}{dt}$$

$$\frac{di_L}{dt} = d \cdot \frac{1}{L}(v_{in} - i_L \cdot (r_{sw} + r_L) - v_o) + d' \cdot \frac{1}{L}(-v_d - (r_d + r_L) i_L - v_o)$$

$$\frac{di_L}{dt} = \frac{1}{L}(dv_{in} - d(r_{sw} + r_L) i_L - dv_o - d' v_d - d'(r_d + r_L) \cdot i_L - d' v_o)$$

$$\frac{d\langle i_L \rangle}{dt} = \frac{1}{L}(d\langle v_{in} \rangle - (dr_{sw} + r_L + d' r_d)\langle i_L \rangle - \langle v_o \rangle - d' v_d)$$

$$\frac{dv_c}{dt} = d \cdot \frac{dv_{c-on}}{dt} + d' \cdot \frac{dv_{c-off}}{dt}$$

$$\frac{dv_{c_{out}}}{dt} = d\left(\frac{1}{r_{c_{out}}C_{out}}v_o - \frac{1}{r_{c_{out}}C_{out}}v_{C_{out}}\right) + d'\left(\frac{1}{r_{c_{out}}C_{out}}v_o - \frac{1}{r_{c_{out}}C_{out}}v_{C_{out}}\right)$$

$$\frac{d\langle v_{c_{out}}\rangle}{dt} = \frac{1}{r_{c_{out}}C_{out}}\langle v_o\rangle - \frac{1}{r_{c_{out}}C_{out}}\langle v_{C_{out}}\rangle$$

$$\frac{dv_{c_{in}}}{dt} = d\left(\frac{1}{r_{c_{in}}C}\left(v_{in} - v_{C_{in}}\right)\right) + d'\left(\frac{1}{r_{c_{in}}C}\left(v_{in} - v_{C_{in}}\right)\right)$$

$$\frac{d\langle v_{c_{in}}\rangle}{dt} = \frac{1}{r_{c_{in}}C_{in}}\langle v_{in}\rangle - \frac{1}{r_{c_{in}}C_{in}}\langle v_{C_{in}}\rangle$$

$$i_{in} = d \cdot i_{in-on} + d' \cdot i_{in-off}$$

$$i_{in} = \mathrm{d}\left(i_L + \frac{1}{r_{c_{in}}}v_{in} - \frac{1}{r_{c_{in}}}v_{C_{in}}\right) + d'\left(\frac{1}{r_{c_{in}}}v_{in} - \frac{1}{r_{c_{in}}}v_{C_{in}}\right)$$

$$\langle i_{in}\rangle = d\langle i_L\rangle + \frac{1}{r_{c_{in}}}\langle v_{in}\rangle - \frac{1}{r_{c_{in}}}\langle v_{C_{in}}\rangle$$

$$i_o = d \cdot i_{o-on} + d' \cdot i_{o-off}$$

$$i_o = d \cdot \left(i_L - \frac{1}{r_{C_{out}}}v_o + \frac{1}{r_{C_{out}}}v_{C_{out}}\right) + d' \cdot \left(i_L - \frac{1}{r_{C_{out}}}v_o + \frac{1}{r_{C_{out}}}v_{C_{out}}\right)$$

$$\langle i_o\rangle = \langle i_L\rangle - \frac{1}{r_{C_{out}}}\langle v_o\rangle + \frac{1}{r_{C_{out}}}\langle v_{C_{out}}\rangle$$

Steady-state operation point:

$$\frac{dv_{c_{in}}}{dt} = \frac{1}{r_{c_{in}}C_{in}}\left(v_{in} - v_{C_{in}}\right)$$

$$0 = \left(V_{in} - V_{C_{in}}\right)$$

$$V_{in} = V_{C_{in}}$$

$$\frac{dv_{c_{out}}}{dt} = \frac{1}{r_{c_{out}}C_{out}}v_o - \frac{1}{r_{c_{out}}C_{out}}v_{C_{out}}$$

$$0 = \frac{1}{r_{c_{out}}C_{out}}V_o - \frac{1}{r_{c_{out}}C_{out}}V_{C_{out}}$$

$$V_o = V_{C_{out}}$$

$$I_{in} = DI_L + \frac{1}{r_{c_{in}}}\mathrm{V}_{in} - \frac{1}{r_{c_{in}}}\mathrm{V}_{c_{in}}$$

$$I_{in} = DI_L$$

$$\mathrm{I}_o = \mathrm{I}_L - \frac{1}{r_{C_{out}}}\mathrm{V}_o + \frac{1}{r_{C_{out}}}V_{C_{out}}$$

$$I_o = I_L$$

$$\frac{di_L}{dt} = \frac{1}{L}(d\langle v_{in}\rangle - (dr_{sw} + r_L + d'r_d)\langle i_L\rangle - \langle v_o\rangle - d'v_d)$$

$$0 = \frac{1}{L}(DV_{in} - DI_L r_{sw} - r_L I_L - D'r_d I_L - V_o - D'v_d)$$

$$DV_{in} - DI_L r_{sw} + DI_L r_d + Dv_d = r_L I_L + r_d I_L + V_o + v_d$$

$$D = \frac{(r_L + r_d)I_L + V_o + v_d}{V_{in} - (r_{sw} - r_d)I_L + v_d}$$

Substituting the steady state values D becomes:

$$D = \frac{(r_L + r_d)I_o + V_o + v_d}{V_{in} - (r_{sw} - r_d)I_o + v_d}$$

Linearization:

$$\frac{di_L}{dt} = \frac{1}{L}(dv_{in} - dr_{sw}i_L - r_L i_L - (1-d)r_d i_L - v_o - (1-d)v_d)$$

$$\frac{d\hat{\imath}_L}{dt} = \frac{1}{L}\left(D\hat{v}_{in} - (Dr_{sw} + r_L + D'r_d)\hat{\imath}_L - \hat{v}_o + (V_{in} - r_{sw}I_o + r_d I_o + v_d)\hat{d}\right)$$

$$\frac{d\hat{\imath}_L}{dt} = \frac{1}{L}\left(D\hat{v}_{in} - R_3\hat{\imath}_L - \hat{v}_o + R_4\hat{d}\right)$$

$$\frac{d\hat{v}_{c_{in}}}{dt} = \frac{1}{r_{c_{in}}C_{in}}\hat{v}_{in} - \frac{1}{r_{c_{in}}C_{in}}\hat{v}_{c_{in}}$$

$$\frac{d\hat{v}_{c_{out}}}{dt} = \frac{1}{r_{c_{out}}C_{out}}\hat{v}_o - \frac{1}{r_{c_{out}}C_{out}}\hat{v}_{C_{out}}$$

$$\hat{\imath}_{in} = D\hat{\imath}_L + \frac{1}{r_{c_{in}}}\hat{v}_{in} - \frac{1}{r_{c_{in}}}\hat{v}_{C_{in}} + I_L\hat{d}$$

$$\hat{\imath}_o = \hat{\imath}_L - \frac{1}{r_{C_{out}}}\hat{v}_o + \frac{1}{r_{C_{out}}}\hat{v}_{C_{out}}$$

In which

$$R_3 = Dr_{sw} + r_L + D'r_d$$

$$R_4 = V_{in} - r_{sw}I_o + r_dI_o + v_d$$

In matrix format:

$$\frac{d}{dt}\begin{bmatrix} \hat{\imath}_L \\ \hat{v}_{C_{in}} \\ \hat{v}_{C_{out}} \end{bmatrix} = \begin{bmatrix} -\frac{R_3}{L} & 0 & -\frac{1}{L} \\ 0 & -\frac{1}{r_{c_{in}}C_{in}} & 0 \\ 0 & 0 & -\frac{1}{r_{c_{out}}C_{out}} \end{bmatrix}\begin{bmatrix} \hat{\imath}_L \\ \hat{v}_{C_{in}} \\ \hat{v}_{C_{out}} \end{bmatrix} + \begin{bmatrix} \frac{D}{L} & -\frac{1}{L} & \frac{R_4}{L} \\ \frac{1}{r_{c_{in}}C_{in}} & 0 & 0 \\ 0 & \frac{1}{r_{c_{out}}C_{out}} & 0 \end{bmatrix}\begin{bmatrix} \hat{v}_{in} \\ \hat{v}_o \\ \hat{d} \end{bmatrix}$$

$$\begin{bmatrix} \hat{\imath}_{in} \\ \hat{v}_o \end{bmatrix} = \begin{bmatrix} D & -\frac{1}{r_{c_{in}}} & 0 \\ 1 & 0 & \frac{1}{r_{C_{out}}} \end{bmatrix}\begin{bmatrix} \hat{\imath}_L \\ \hat{v}_{C_{in}} \\ \hat{v}_{C_{out}} \end{bmatrix} + \begin{bmatrix} \frac{1}{r_{c_{in}}} & 0 & I_o \\ 0 & -\frac{1}{r_{C_{out}}} & 0 \end{bmatrix}\begin{bmatrix} \hat{v}_{in} \\ \hat{v}_o \\ \hat{d} \end{bmatrix}$$

$$\boldsymbol{A} = \begin{bmatrix} -\frac{R_3}{L} & 0 & -\frac{1}{L} \\ 0 & -\frac{1}{r_{c_{in}}C_{in}} & 0 \\ 0 & 0 & -\frac{1}{r_{c_{out}}C_{out}} \end{bmatrix}, \boldsymbol{B} = \begin{bmatrix} \frac{D}{L} & -\frac{1}{L} & \frac{R_4}{L} \\ \frac{1}{r_{c_{in}}C_{in}} & 0 & 0 \\ 0 & \frac{1}{r_{c_{out}}C_{out}} & 0 \end{bmatrix}$$

$$\boldsymbol{C} = \begin{bmatrix} D & -\frac{1}{r_{c_{in}}} & 0 \\ 1 & 0 & \frac{1}{r_{C_{out}}} \end{bmatrix}, \boldsymbol{D} = \begin{bmatrix} \frac{1}{r_{c_{in}}} & 0 & I_o \\ 0 & -\frac{1}{r_{C_{out}}} & 0 \end{bmatrix}$$